



Mehdikhani, M., Petrov, N. A., Straumit, I., Melro, A. R., Lomov, S. V., & Gorbatiikh, L. (2019). The effect of voids on matrix cracking in composite laminates as revealed by combined computations at the micro- and meso-scales. *Composites Part A: Applied Science and Manufacturing*, 117, 180-192.  
<https://doi.org/10.1016/j.compositesa.2018.11.009>

Peer reviewed version

License (if available):  
CC BY-NC-ND

Link to published version (if available):  
[10.1016/j.compositesa.2018.11.009](https://doi.org/10.1016/j.compositesa.2018.11.009)

[Link to publication record in Explore Bristol Research](#)  
PDF-document

This is the author accepted manuscript (AAM). The final published version (version of record) is available online via Elsevier at <https://www.sciencedirect.com/science/article/pii/S1359835X18304421> . Please refer to any applicable terms of use of the publisher.

## University of Bristol - Explore Bristol Research

### General rights

This document is made available in accordance with publisher policies. Please cite only the published version using the reference above. Full terms of use are available:  
<http://www.bristol.ac.uk/red/research-policy/pure/user-guides/ebr-terms/>

## The effect of voids on matrix cracking in composite laminates as revealed by combined computations at the micro- and meso-scales

Mahoor Mehdikhani <sup>a,b,\*1</sup>, Nikolay A. Petrov <sup>a,1</sup>, Ilya Straumit <sup>a</sup>, António R. Melro <sup>c</sup>, Stepan V. Lomov <sup>a,b</sup>, and Larissa Gorbatikh <sup>a,b</sup>

<sup>a</sup> KU Leuven, Department of Materials Engineering, Kasteelpark Arenberg 44, 3001, Leuven, Belgium

<sup>b</sup> SIM vzw, Technologiepark 935, B-9052 Zwijnaarde, Belgium

<sup>c</sup> Bristol Composites Institute (ACCIS), University of Bristol, Bristol, UK

### Abstract

Voids are an important type of manufacturing defects in fiber-reinforced composites. Matrix cracking is sensitive to the presence of voids. Although this cracking occurs at the ply scale, its dynamics is strongly affected by ply's microstructure, in particular, fiber distribution, fiber content, and the presence of voids. In the current study, a computational approach to simulate the influence of intra-laminar voids on cracking in composite laminates is developed. The approach combines finite element models of two scales: a micro-scale model, where the fibers and voids are modeled explicitly, and a meso-scale model, where the cracking phenomenon is captured on the ply scale. The micro-scale model, incorporating plasticity and damage in the matrix, provides input for the meso-scale model, which simulates the progressive cracking by means of the extended finite element method. The methodology is applied to investigate the effect of voids on the density of transverse cracks in cross-ply laminates in function of the quasi-static tensile load. Different sizes and contents of voids, which are chosen based on experimental micro-computed tomography data, are simulated. The numerical experiments show that the presence of voids leads to earlier start of the cracking, with the crack density evolution less sensitive to voids.

**Keywords:** B. Porosity; B. Transverse cracking; C. Finite element analysis (FEA); Multiscale modeling

\*Corresponding author E-mail: [mahoor.mehdikhani@kuleuven.be](mailto:mahoor.mehdikhani@kuleuven.be)

<sup>1</sup> These authors contributed equally to this work

---

## 1 Introduction

Being defined as “regions unfilled with polymer and fibers” [1], voids are an important type of manufacturing defects in Fiber-Reinforced Composites (FRCs). Although there is a vast amount of research on voids and their effects on the mechanical behavior of FRCs, starting from the 1960s, it remains an intensively studied topic. A detailed review of the state-of-the-art on the voids' formation, characteristics, and effects on

1 mechanical performance of FRCs can be found in [1]; early research is summarized in [2]. According to [1],  
2 voids are still important due to 1) the remaining unknowns about their mechanical influence, 2) being a central  
3 issue in modern manufacturing techniques, such as out-of-autoclave curing and automated prepreg laying, 3)  
4 becoming a point of concern in manufacturing of modern aeronautical parts with ever increasing geometrical  
5 complexity and modified resins, and 4) high costs associated with their removal during or repair after  
6 production, while a “void-free” composite is often not needed. As stressed in [3], modeling methods are  
7 needed to quantify the influence of voids on mechanical behavior of composites, which would allow definition  
8 of adequate allowance limits for design with “as manufactured” materials.  
9

10 Voids are found to significantly degrade the matrix- and interface-dominated mechanical properties,  
11 whereas fiber-dominated properties show lower sensitivity to their presence [4-6]. Void content, a  
12 manufacturing quality parameter, is traditionally used for evaluation of the mechanical effects of voids.  
13 Nevertheless, recent studies, including [7-10], have shown that solely evaluating void content is not sufficient  
14 in the analysis of voids’ effects because it is a global parameter and provides no data on locally critical voids  
15 that can lead to (premature) failure. Hence, other void characteristics, i.e. shape, size, location, and  
16 distribution, also must be taken into account. This is mainly achieved by performing simulations [11] and  
17 micro-scale experiments, using such tools as X-ray micro-Computed Tomography (micro-CT) [8] and micro-  
18 scale digital image correlation [12, 13], which are increasingly popular in the investigation of voids’ effects.  
19

20 One of the first damage modes occurring in composite laminates under thermo-mechanical loading is  
21 formation of matrix cracks running through the ply thickness and width (in the fiber direction). Although the  
22 cracking in off-axis plies is not the final failure mechanism in FRCs, it does induce other failure modes such as  
23 inter-laminar cracks (delamination) and fiber breakage, leading to the final failure of the laminate [14]. In  
24 cross-ply laminates, the matrix cracks in the 90° plies are called “transverse” cracks. The onset strain, the  
25 density growth rate, and the saturation density level are controlled by many parameters including ply  
26 thickness, laminate stacking sequence, properties of the fibers, matrix, and interface as well as by the volume  
27 fraction and distribution of the fibers. The transverse cracking is also sensitive to the presence of  
28 manufacturing defects such as intra-laminar voids, i.e. the subject of the present paper.  
29

30 In the last five years, the interest in understanding the effect of voids on matrix cracking in FRCs has  
31 increased. For cross-ply carbon/epoxy laminates [15] and quasi-isotropic laminates of non-crimp-fabric  
32 carbon/epoxy plies [16], it was reported that voids have a more significant effect on the initial stages of  
33 cracking than on the final (saturation) stage. According to [15], this is because voids trigger the formation of  
34

1 initial matrix cracks in off-axis plies, but with the increase of the global loading, their effect on further  
2 cracking diminishes since fewer and fewer voids remain without cracks. This can be a reason for the random  
3 formation of initial cracks (from random voids) and a more uniform distribution with the increase of the  
4 loading [17]. It was observed that voids have a larger influence on matrix cracking in 90° plies than in 45°  
5 plies [16], which motivates the investigation of voids' effect on matrix cracking in cross-ply laminates.  
6 Performing a micro-scale digital image correlation in [12], the authors noted that voids create strain  
7 concentrations, leading to local plastic deformation of the matrix, causing earlier matrix failure. The strain  
8 concentration factor around a real-shape void was calculated numerically in [9] and correlated with the global  
9 strain to crack initiation. The initiation of cracks from voids in a cross-ply carbon/epoxy laminate was  
10 confirmed by a micro-scale *in-situ* analysis performed inside an electron microscope in [18], where the  
11 combined effect of voids and matrix cure degree on evolution of transverse cracking was investigated, using  
12 digital image correlation, also at the meso- and macro-scales.

13  
14  
15  
16  
17  
18  
19  
20  
21  
22  
23 Despite many noteworthy results, the available studies focus either on local analysis of voids or on their  
24 global influence and miss the link between the two. This link is, however, important as intra-laminar voids are  
25 micro-scale features, which interact with other heterogeneities in the material both at lower and higher scales  
26 such as fibers at the micro-scale and cracks at the meso-scale (the ply/laminate scale). Therefore, in evaluation  
27 and prediction of the effect of voids on statistically controlled properties, such as matrix cracking, one is  
28 confronted with the scale issue and needs an approach that would combine both scales.

29  
30  
31  
32  
33  
34  
35 Modeling of damage in laminated composites (the scale of millimeters) with direct representation of fibers  
36 (the scale of micrometers) requires significant computational resources and is feasible only in 2D formulation  
37 [19]. Today, such an approach in 3D would be difficult to realize even with the help of high-performance  
38 computer clusters. Attempts to bypass the challenge of scales may lead to unphysical representation of  
39 modeled phenomena, which is the case in [20] where meso-scale damage parameters are identified using  
40 micro-scale models without considering the important scale difference. The approach in [20] may be  
41 acceptable for materials exhibiting distributed micro-damage (like fiber/matrix debonding) but loses its  
42 adequacy for laminates with discrete damage such as ply cracking.

43  
44  
45  
46  
47  
48  
49  
50  
51 An alternative approach that is physically sound and yet computationally affordable is the one where  
52 models of different scales are linked together. This multiscale computational approach [21] relies on already  
53 developed models for each individual scale. For example, the transverse cracking (in the absence of voids) can  
54 be modeled using fracture mechanics approach [22] or eXtended Finite Element Method (XFEM) [23-25]. The  
55  
56  
57  
58  
59  
60  
61

latter requires knowledge of the cohesive behavior of damaged elements, often linked to physical characteristics such as strength and fracture toughness of the ply material. The strength and fracture toughness can be evaluated experimentally or predicted using micromechanical models [26, 27]. In [28], the two scales are bridged by assessing crack initiation using stress concentrations at the micro-scale, and calculating the cracking evolution under fatigue loading using an empirical Paris-like law for the crack growth.

All the studies, referenced in the last two paragraphs, deal with materials free of voids. When voids are present, and the aim is to understand correlations between the void characteristics and the crack density evolution, the link between the micro- and meso-scale analyses becomes even more critical. This is because of an additional scale factor, namely the characteristic length related to the voids' size and spatial distribution (as mentioned above). Therefore, a multiscale approach is required to predict the effect of voids on the cracking evolution.

The present study proposes a numerical two-scale modeling approach to analyze the effect of intra-laminar voids on the evolution of transverse cracks with applied strain. This approach accounts for the complexity of different length scales being present and interacting. In the micro-model, these length scales are related to the fiber size, density of the fiber packing, and void size; in the transition to the meso-model, the length scales are related to the void content and voids' spatial distribution; and in the meso-model, the length scale is linked to the crack spacing and its evolution.

## 2 Combined two-scale approach

### 2.1 Methodology

A  $[0^\circ/90^\circ/0^\circ]$  laminate, consisting of unidirectional (UD) fibrous plies with a given fiber volume fraction, and under tensile loading in the  $0^\circ$  direction is modeled. The  $90^\circ$  ply (called also “transverse ply”) contains voids. Based on the void characterization results (Section 2.2), the voids are assumed to have an elongated shape and to be oriented in the fiber direction. This is because in this type of materials, voids are typically the remaining dry volumes between the fibers. The void content, voids' spatial distribution, and statistics of the voids' size and aspect ratio are given (either varied or assumed constant). The aim of the calculation is simulation of the effect of voids on the cracking process in the  $90^\circ$  ply. The focus of this study is on challenges in prediction of void-sensitivity of transverse cracking and the subsequent damage mechanisms such as delamination are not considered at this stage.

Fig. 1 illustrates schematically the steps of the modeling methodology:

1 *Step 1. Micro-scale modeling.* A 3D Representative Defective Volume (RDV) of a transverse ply with a  
2 void (“defective” ply) is modeled at the micro-scale, along with the Representative Volume Element (RVE) of  
3 the “pristine” (reference) ply. The fibers are assumed transversely isotropic elastic bodies, all aligned in one  
4 direction, and randomly distributed within the plane of isotropy. The matrix is modeled to account for  
5 plasticity and pressure-dependent progressive damage [26]. The effective properties of the defective and of the  
6 pristine material are computed using Finite Element (FE) method: stiffness matrix, strength under transverse  
7 tensile loading, and Mode I fracture toughness. These properties are also referred to as “effective properties”  
8 of the defective and pristine materials.  
9

10 *Step 2. Scale transition.* The effective properties are transferred to a 3D meso-scale FE model of the cross-  
11 ply laminate, serving as material parameters for “weak volumes”, which represent voids’ loci. The weak  
12 volumes are distributed randomly in the transverse ply, according to a given void content, size, and aspect ratio  
13 as well as voids’ spatial distribution and orientation. The cross-sectional size of the weak volume corresponds  
14 to the size of the study region in the micro-scale model, for which effective properties are calculated.  
15

16 *Step 3. Meso-scale modeling.* XFEM is utilized to model the [onset and development](#) of transverse cracking  
17 in the 90° ply of the laminate under tensile loading.  
18

## 19 2.2 Identification of typical void characteristics

20 For acquiring realistic data on void characteristics to be used in simulations, micro-CT was performed on a  
21 [0/90]<sub>4s</sub> carbon/epoxy laminate, produced through automated tape laying and autoclave curing at *SABCA*  
22 *Limburg NV*, Belgium. Intra-laminar voids suitable for this study were intentionally introduced to the laminate  
23 by means of the “low pressure cured debulked” processing, as described in [29]. The micro-CT was performed  
24 with the *HECTOR* system [30], from *Ghent University Centre for X-ray Tomography (UGCT)*. The images  
25 were captured with a resolution of 6.55 μm/pixel, reconstructed in *Octopus* software and segmented via  
26 *VoxTex* software [31]. The post-processing was performed in a volume of ~ 10 mm × 10 mm × 3 mm inside  
27 the sample. [Micro-CT analysis of a similar material, only with a different cure cycle \(the manufacturer’s](#)  
28 [recommended cycle\), does not show any voids, as investigated in \[32\].](#)  
29

30 The detected voids have elongated shapes (Fig. 2a), and their cross-sectional shape is irregular. For  
31 analysis of void characteristics, each void is fitted to an ellipsoid with three size parameters: major axis,  
32 middle axis, and minor axis. The cross-section size is evaluated with the geometric mean of the transversal  
33 axes, which are the middle and minor axes, as defined in Fig 2b. Moreover, for each void, a “roundness  
34 factor”, i.e. the ratio of the minor and middle axes, and an “elongation factor”, i.e. the ratio of the major and  
35

1 the geometric mean of the transversal axes, is defined. The orientation of the voids is quantified with the angle  
2 between their major axis and the scan direction. The latter is close (within few degrees) to the  $0^\circ$  direction of  
3 the laminate. There are some detected features, of which the minor axis is below  $8\ \mu\text{m}$  and the orientation is an  
4 exact number. They seem to be false features due to creating non-physical clusters in the frequency  
5 distribution graphs, so they are filtered out. Relative frequency distribution graphs of all the described  
6 parameters are illustrated in Fig. 2. Around half of the voids have a geometric mean of the transversal axes  
7 between  $20$  and  $60\ \mu\text{m}$  and a major axis (length) between  $100$  and  $1000\ \mu\text{m}$ . The results show that more than  
8 half of the voids have a roundness factor above  $0.6$  (Fig. 2d) and an elongation factor above  $6$  (Fig. 2e).  
9 Furthermore, most of the voids are aligned with the fibers in each UD ply (Fig. 2f).

10  
11  
12  
13  
14  
15  
16  
17 The results of the micro-CT characterization were used to guide the choice of void characteristics and to  
18 motivate simplifications in the simulations. For the sake of simplicity, the voids are assumed to have circular  
19 cross-sections. The fact that more than half of the voids have a roundness factor above  $0.6$  makes this  
20 assumption justifiable. Of course, once the modeling methodology is established, the effect of void's shape can  
21 be investigated, but it is out of the scope of the current study. The typical voids morphology is characterized  
22 by large elongation factor. Therefore, the voids in the micro-model are assumed sufficiently long to the extent  
23 that the plain strain condition can be applied. The actual length of the voids is assumed to be  $1000\ \mu\text{m}$  (as an  
24 upper bound estimate) and is introduced in the meso-model. In order to study the effect of void cross-section  
25 size, two cases are investigated based on the micro-CT results of the transversal axes mean: small ( $30\ \mu\text{m}$ ) and  
26 large voids ( $60\ \mu\text{m}$ ). The former is close to the average transversal axes mean of the measured voids (i.e.  $27$   
27  $\mu\text{m}$ ) and the latter represents the case of the largest voids.  $95\%$  of voids have a transversal axes mean below  $60$   
28  $\mu\text{m}$ .

### 29 2.3 Micro-scale modeling

30  
31  
32  
33  
34  
35  
36  
37  
38  
39  
40  
41  
42  
43  
44  
45  
46  
47  
48  
49  
50  
51  
52  
53  
54  
55  
56  
57  
58  
59  
60  
61  
62  
63  
64  
65  
66  
67  
68  
69  
70  
71  
72  
73  
74  
75  
76  
77  
78  
79  
80  
81  
82  
83  
84  
85  
86  
87  
88  
89  
90  
91  
92  
93  
94  
95  
96  
97  
98  
99  
100  
101  
102  
103  
104  
105  
106  
107  
108  
109  
110  
111  
112  
113  
114  
115  
116  
117  
118  
119  
120  
121  
122  
123  
124  
125  
126  
127  
128  
129  
130  
131  
132  
133  
134  
135  
136  
137  
138  
139  
140  
141  
142  
143  
144  
145  
146  
147  
148  
149  
150  
151  
152  
153  
154  
155  
156  
157  
158  
159  
160  
161  
162  
163  
164  
165  
166  
167  
168  
169  
170  
171  
172  
173  
174  
175  
176  
177  
178  
179  
180  
181  
182  
183  
184  
185  
186  
187  
188  
189  
190  
191  
192  
193  
194  
195  
196  
197  
198  
199  
200  
201  
202  
203  
204  
205  
206  
207  
208  
209  
210  
211  
212  
213  
214  
215  
216  
217  
218  
219  
220  
221  
222  
223  
224  
225  
226  
227  
228  
229  
230  
231  
232  
233  
234  
235  
236  
237  
238  
239  
240  
241  
242  
243  
244  
245  
246  
247  
248  
249  
250  
251  
252  
253  
254  
255  
256  
257  
258  
259  
260  
261  
262  
263  
264  
265  
266  
267  
268  
269  
270  
271  
272  
273  
274  
275  
276  
277  
278  
279  
280  
281  
282  
283  
284  
285  
286  
287  
288  
289  
290  
291  
292  
293  
294  
295  
296  
297  
298  
299  
300  
301  
302  
303  
304  
305  
306  
307  
308  
309  
310  
311  
312  
313  
314  
315  
316  
317  
318  
319  
320  
321  
322  
323  
324  
325  
326  
327  
328  
329  
330  
331  
332  
333  
334  
335  
336  
337  
338  
339  
340  
341  
342  
343  
344  
345  
346  
347  
348  
349  
350  
351  
352  
353  
354  
355  
356  
357  
358  
359  
360  
361  
362  
363  
364  
365  
366  
367  
368  
369  
370  
371  
372  
373  
374  
375  
376  
377  
378  
379  
380  
381  
382  
383  
384  
385  
386  
387  
388  
389  
390  
391  
392  
393  
394  
395  
396  
397  
398  
399  
400  
401  
402  
403  
404  
405  
406  
407  
408  
409  
410  
411  
412  
413  
414  
415  
416  
417  
418  
419  
420  
421  
422  
423  
424  
425  
426  
427  
428  
429  
430  
431  
432  
433  
434  
435  
436  
437  
438  
439  
440  
441  
442  
443  
444  
445  
446  
447  
448  
449  
450  
451  
452  
453  
454  
455  
456  
457  
458  
459  
460  
461  
462  
463  
464  
465  
466  
467  
468  
469  
470  
471  
472  
473  
474  
475  
476  
477  
478  
479  
480  
481  
482  
483  
484  
485  
486  
487  
488  
489  
490  
491  
492  
493  
494  
495  
496  
497  
498  
499  
500  
501  
502  
503  
504  
505  
506  
507  
508  
509  
510  
511  
512  
513  
514  
515  
516  
517  
518  
519  
520  
521  
522  
523  
524  
525  
526  
527  
528  
529  
530  
531  
532  
533  
534  
535  
536  
537  
538  
539  
540  
541  
542  
543  
544  
545  
546  
547  
548  
549  
550  
551  
552  
553  
554  
555  
556  
557  
558  
559  
560  
561  
562  
563  
564  
565  
566  
567  
568  
569  
570  
571  
572  
573  
574  
575  
576  
577  
578  
579  
580  
581  
582  
583  
584  
585  
586  
587  
588  
589  
590  
591  
592  
593  
594  
595  
596  
597  
598  
599  
600  
601  
602  
603  
604  
605  
606  
607  
608  
609  
610  
611  
612  
613  
614  
615  
616  
617  
618  
619  
620  
621  
622  
623  
624  
625  
626  
627  
628  
629  
630  
631  
632  
633  
634  
635  
636  
637  
638  
639  
640  
641  
642  
643  
644  
645  
646  
647  
648  
649  
650  
651  
652  
653  
654  
655  
656  
657  
658  
659  
660  
661  
662  
663  
664  
665  
666  
667  
668  
669  
670  
671  
672  
673  
674  
675  
676  
677  
678  
679  
680  
681  
682  
683  
684  
685  
686  
687  
688  
689  
690  
691  
692  
693  
694  
695  
696  
697  
698  
699  
700  
701  
702  
703  
704  
705  
706  
707  
708  
709  
710  
711  
712  
713  
714  
715  
716  
717  
718  
719  
720  
721  
722  
723  
724  
725  
726  
727  
728  
729  
730  
731  
732  
733  
734  
735  
736  
737  
738  
739  
740  
741  
742  
743  
744  
745  
746  
747  
748  
749  
750  
751  
752  
753  
754  
755  
756  
757  
758  
759  
760  
761  
762  
763  
764  
765  
766  
767  
768  
769  
770  
771  
772  
773  
774  
775  
776  
777  
778  
779  
780  
781  
782  
783  
784  
785  
786  
787  
788  
789  
790  
791  
792  
793  
794  
795  
796  
797  
798  
799  
800  
801  
802  
803  
804  
805  
806  
807  
808  
809  
810  
811  
812  
813  
814  
815  
816  
817  
818  
819  
820  
821  
822  
823  
824  
825  
826  
827  
828  
829  
830  
831  
832  
833  
834  
835  
836  
837  
838  
839  
840  
841  
842  
843  
844  
845  
846  
847  
848  
849  
850  
851  
852  
853  
854  
855  
856  
857  
858  
859  
860  
861  
862  
863  
864  
865  
866  
867  
868  
869  
870  
871  
872  
873  
874  
875  
876  
877  
878  
879  
880  
881  
882  
883  
884  
885  
886  
887  
888  
889  
890  
891  
892  
893  
894  
895  
896  
897  
898  
899  
900  
901  
902  
903  
904  
905  
906  
907  
908  
909  
910  
911  
912  
913  
914  
915  
916  
917  
918  
919  
920  
921  
922  
923  
924  
925  
926  
927  
928  
929  
930  
931  
932  
933  
934  
935  
936  
937  
938  
939  
940  
941  
942  
943  
944  
945  
946  
947  
948  
949  
950  
951  
952  
953  
954  
955  
956  
957  
958  
959  
960  
961  
962  
963  
964  
965  
966  
967  
968  
969  
970  
971  
972  
973  
974  
975  
976  
977  
978  
979  
980  
981  
982  
983  
984  
985  
986  
987  
988  
989  
990  
991  
992  
993  
994  
995  
996  
997  
998  
999  
1000

total are created, which are called hereafter “*Micro-Ref-S*”, “*Micro-Void-S*”, “*Micro-Ref-L*”, and “*Micro-Void-L*”, where *Ref* means *Reference*, and *S* and *L* stand for *Small* and *Large* void size, respectively. The [micro-scale](#) modeling is performed using the commercial FE software *Abaqus 6.13* and its implicit solver. Although a higher number of RVEs and RDVs would provide more data for statistical analysis of the strength, one RVE and RDV for each case would be sufficient for this study since the statistical variation of strength caused by difference in fiber distribution is negligible when compared to the variation caused by voids, as seen in Table 1.

### 2.3.1 Model size

The two void sizes selected in Section 2.2 are considered for the diameter of the circular void in micro-modeling. For each void-size case, the void is placed in the center of the RDV, and the RDV cross-sectional size is chosen such that the void is sufficiently far from the RDV edges. This ensures that interaction between the void and the model edges is negligible. This distance is estimated using an analytical solution for tension of a homogenous plate with a circular hole in the center. Based on this solution, at a distance of 3.5 times the hole diameter from the hole center, the stress concentration caused by the hole is less than 5%. Thus, the RDV size is chosen as 7 times of the void diameter for each case. For the sake of computational cost, only one half of each RDV is modeled and symmetric Boundary Conditions (BCs) are applied. To further reduce the computational cost, the size of the RDV in the fiber direction is selected as a small value, i.e. 0.15 times the fiber radius, where fiber radius is 3.5  $\mu\text{m}$ . Applying symmetric BCs in the fiber direction, plane strain conditions are simulated (Section 2.3.4). The RVE size is the same as its corresponding RDV size for each void size. Therefore, the RVE and RDV size for the 30- $\mu\text{m}$ -diameter void is 210  $\mu\text{m} \times 105 \mu\text{m} \times 0.525 \mu\text{m}$ , and for the 60- $\mu\text{m}$ -diameter void is 420  $\mu\text{m} \times 210 \mu\text{m} \times 0.525 \mu\text{m}$ . The RVEs and RDVs with their sizes are shown in Fig. 3.

### 2.3.2 Fiber distribution

The fibers are uniformly randomly distributed inside each model, using the algorithm developed in [33] and investigated versus real microstructures in [34]. The target fiber volume fraction is 58%, and the low and high bounds for minimum distance between the centers of fibers are 2.05 and 2.2 times the fiber radius, respectively. All the fibers that fall on the model edges are manually repositioned to have them exactly halved. This is performed to allow a physically correct application of symmetric BCs. Such fiber repositioning has a negligible effect on the modeling results since three of the four edges are excluded in post-processing. In addition to this, for the cases with a void, i.e. *Micro-Void-S* and *Micro-Void-L*, the fibers, overlapping the void,



are either removed or manually repositioned to fill the area surrounding the void, depending on the size of the unoccupied matrix region around the void. In some cases, there was a need for small repositioning of the neighboring fibers as well. Although the overall fiber volume fraction remains similar for the cases with and without a void, this adjustment of the fiber positioning causes a small increase in the local fiber volume fraction around the void, which can also occur in reality since voids may push the surrounding fibers away [5]. The final fiber volume fraction of all the cases is within 57-58% (shown for each model in Table 1).

### 2.3.3 Material models for the constituents

There are three constituents modeled in the micro-modeling: carbon fibers, epoxy matrix, and voids. Carbon fibers (*AS4* from *Hexcel*) are modeled as a transversely isotropic material, with properties taken from [19]. Their longitudinal elastic modulus, transverse elastic modulus, in-plane Poisson's ratio, out-of-plane Poisson's ratio, and in-plane shear modulus are respectively 232 GPa, 13.0 GPa, 0.30, 0.46, and 11.3 GPa. Voids are modeled as an isotropic material with extremely low mechanical properties (not zero to avoid instability in computations), namely  $10^{-6}$  for both Young's modulus (in GPa) and Poisson's ratio.

Matrix is simulated with a continuum model for an epoxy material as characterized in [35] and used in [26, 27]. Its elastic modulus, Poisson's ratio, plastic Poisson's ratio, tensile strength, and fracture toughness are 3.9 GPa, 0.39, 0.30, 93.0 MPa, and  $90 \text{ J/m}^2$  (0.09 N/mm), respectively. The continuum model, developed in [26] and applied in [27], is a constitutive pressure-dependent model, and accounts for linear elasticity, plasticity, and progressive damage of the matrix. The yield is described by the paraboloid yield criterion presented in [36]. Hardening is considered with an increase in equivalent plastic strain both under tension and compression. For this, experimental stress-strain data from [35] are fed to the model. The matrix damage is considered to be isotropic and modeled based on the thermodynamics approach. Damage input parameters are tensile strength and Mode I fracture toughness. More details of the matrix model can be found in [26]. This model is implemented as a User-defined MATerial model (*UMAT*) user subroutine in the *Abaqus* software.

The interface between fibers and matrix is assumed to be perfect. The focus of this study is development of a methodology for analysis of the effect of voids, and the number of influencing parameters is intentionally kept to a minimum. Of course, once the methodology is established, one can explore the effect of many parameters including interfacial strength and fracture energy.

### 2.3.4 Mesh and boundary conditions

The 3D micro-models are discretized with *Hex-dominated* control, which causes ~ 4% of the elements to become wedge elements (C3D6), and the rest to have hexahedral shape (C3D8R). In order to have a finer

1 mesh on the fiber/matrix interfaces, they were seeded with a size half of that on the model edges. The element  
2 size on the fiber/matrix interfaces is  $\sim 0.4 \mu\text{m}$ . The models have only one element in the fiber direction. The  
3 total number of elements in the small models (*Micro-Ref-S* and *Micro-Void-S*) is  $\sim 111000$ , and in the large  
4 models (*Micro-Ref-L* and *Micro-Void-L*) is  $\sim 472000$ . The mesh independency of the micro-scale model is  
5 explored in [26].  
6  
7

8  
9 To calculate effective elastic properties ( $E_L$ ,  $E_T$ ,  $\nu_{LT}$ ,  $\nu_{TT}$ ,  $G_{TT}$ ), which will be used in the meso-modeling,  
10 elastic homogenization is performed, considering no damage and plasticity for the matrix. Assuming  
11 transverse isotropy, three separate sets of BCs (tensile loading in three directions) are applied to each micro-  
12 model, as described in [37]. Then, the uniaxial transverse tension problem is considered to model failure.  
13 Transverse tension is applied to the models by exerting constant displacements to the left and right edges. In  
14 the other two directions, i.e. fiber direction and the other transverse direction, Poisson's contraction is  
15 prescribed through constant displacements, calculated based on the effective elastic properties of the ply, using  
16 analytical formulas of Chamis [38] for each case. For example, the effective properties calculated for *Micro-  
17 Ref-S* with a fiber volume fraction of 57.6% are as follows: the longitudinal elastic modulus, transverse elastic  
18 modulus, in-plane Poisson's ratio, out-of-plane Poisson's ratio, and in-plane shear modulus are respectively  
19 135 GPa, 8.3 GPa, 0.34, 0.42, and 4.2 GPa. To help with the convergence of the damage models, stabilization  
20 and automatic damping are applied. Since only the local properties of the material, in the presence and absence  
21 of voids, are calculated using the micro-scale models (and not the global properties), periodic BCs (of which  
22 some examples can be found in [33, 39, 40]) could also be applied instead of symmetric BCs.  
23  
24  
25  
26  
27  
28  
29  
30  
31  
32  
33  
34  
35  
36

### 37 2.3.5 Post-processing: calculation of the effective properties

38  
39 The results of the micro-modeling include (a) stress-strain fields in the elastic regime of loading and (b)  
40 stress-strain history during loading until full formation of the transverse matrix crack and load drop to zero.  
41 The matrix crack is seen in Fig. 3 as the elements with a "damage variable" of 1 (fully damaged). These results  
42 are processed to obtain the properties of the defective and pristine materials needed for the meso-model. This  
43 processing accounts for the size effect in the defective material: effective properties of a volume containing a  
44 void with a given size depend on the size of the volume. Therefore, three regions are defined in the micro-  
45 models for calculation of the effective properties. The regions' sizes are referred to below as rectangles  $X \times Y$   
46 around half a void (Fig. 3), which correspond to  $X \times 2Y$  rectangles around the full void (due to symmetric  
47 BCs).  
48  
49  
50  
51  
52  
53  
54  
55  
56  
57  
58  
59  
60  
61  
62  
63  
64  
65

Regions for calculation of elastic properties (*E*-regions in Fig. 3). The micro-model resulting elastic properties will be used in the meso-models to represent effective properties of the pristine material and reduction of elastic properties of the defective material. The homogenization is performed on different regions of the micro-models with different fiber and void volume fractions. For the pristine material, this region is *E-Ref-S*, which comprises the full volume of *Micro-Ref-S* (Fig. 3a). For the defective material, two regions are defined to represent two values of the void content (1.6% and 5%) in each of the *Micro-Void-S* and *Micro-Void-L* models. The full volume of the micro-models corresponds to the void content of 1.6%; it has a size of  $210\ \mu\text{m} \times 105\ \mu\text{m}$  (region *E-S-Low%*) in *Micro-Void-S* and  $420\ \mu\text{m} \times 210\ \mu\text{m}$  (region *E-L-Low%*) in *Micro-Void-L* (Fig. 3b and e, respectively). Regions, corresponding to the void content of 5%, have dimensions of  $119\ \mu\text{m} \times 59.5\ \mu\text{m}$  (region *E-S-High%*) and  $238\ \mu\text{m} \times 119\ \mu\text{m}$  (region *E-L-High%*) respectively in *Micro-Void-S* and *Micro-Void-L* and are respectively shown in Fig. 3b and e as red rectangles.

Regions for calculation of damage-related properties (*D*-regions in Fig. 3). These properties are transverse strength and Mode I fracture toughness to be used as parameters of the cohesive law, used for prediction of ply cracking. The region has the size  $100\ \mu\text{m} \times 35\ \mu\text{m}$ , corresponding (accounting for the symmetry) to a  $100\ \mu\text{m} \times 70\ \mu\text{m}$  rectangle around the void. It is called *D-Ref-S*, *D-S*, and *D-L* in *Micro-Ref-S*, *Micro-Void-S*, and *Micro-Void-L*, respectively (dashed and solid black rectangles in Fig. 3a, b, and e respectively). Fig. 3c and f show the micro-model resulting tension diagrams, presenting dependency of the transverse effective stress on the transverse effective strain calculated for all the micro-scale models and different post-processing regions. Further processing of these curves and extraction of the material properties used in the meso-scale modeling is described in Section 2.4.3. **If the void content is high enough to have significant interaction of the neighboring voids, affecting the damage development in their vicinity, the micro-model should include multiple voids to reflect this interaction. However, the current model does not account for this effect, which is an approximation based on the relatively low void contents.**

#### 2.4 Meso-scale modeling

Five meso-scale models, all with  $[0^\circ/90^\circ/0^\circ]$  stacking sequence, are created for analysis of transverse cracking: the reference model without voids, the models with small (30- $\mu\text{m}$  transversal axes mean) and large (60- $\mu\text{m}$  transversal axes mean) ellipsoidal voids, with the global void content, in each case, at two levels: 1.6% (low) and 5% (high). The meso-models are called hereafter: “*Meso-S-Low%*”, “*Meso-S-High%*”, “*Meso-L-Low%*”, “*Meso-L-High%*”, and “*Meso-Ref*”, where *S* and *L* stand for *Small* and *Large* void sizes, respectively,

and *Ref* for the case without voids. The meso-scale modeling is performed in *Abaqus 2017*, using its implementation of the XFEM, and its implicit solver.

The XFEM allows modeling of initiation and propagation of multiple cracks in certain areas of the model, where elements are enriched by adding extra degrees of freedom to the nodes. Those areas are referred to hereafter as “enriched” regions. *Abaqus 2017* imposes restrictions on the definition of the enrichments: there should be at least two non-enriched elements between two successive enriched regions, and the total number of enriched regions in the model cannot exceed 100. For more detailed discussion on how the XFEM works in application to cracking in composites, the reader is referred to [25].

#### 2.4.1 Geometry, mesh, and boundary conditions

Each 3D meso-scale model simulates a  $[0^\circ/90^\circ/0^\circ]$  specimen that is 20 mm in both width and length and made of plies with 0.21 mm thickness (Fig. 4a). The coordinates’ notation is as follows: *Z* coordinate corresponds to the  $0^\circ$  direction, *X* to the  $90^\circ$  and *Y* to the thickness direction. The model is meshed such that each ply has 3 elements through the ply thickness, 100 elements along the width, and 300 elements along the length direction (Fig. 4b). The transverse ply has 100 enriched regions (the maximum admissible number), each occupying one element in the laminate length direction, the full width, and the full thickness of the middle ply. They are aligned in the width direction and evenly spaced along the laminate length with two non-enriched elements in between (Fig. 4b). There are two sizes of elements:  $100\ \mu\text{m} \times 70\ \mu\text{m} \times 200\ \mu\text{m}$  and  $50\ \mu\text{m} \times 70\ \mu\text{m} \times 200\ \mu\text{m}$  respectively in the *Z*, *Y*, and *X* directions. All elements of the XFEM-enriched regions have the former size, while the latter size is used for the elements between the enriched regions. Mesh sensitivity for XFEM solution was studied in [25]. For convergence of the model, viscous regularization is applied to stabilize the response during damage. The numerical viscosity value is chosen such that it has negligible influence on the XFEM cohesive behavior.

The BCs for the meso-model are as follows. Tensile displacement along the *Z*-axis, equivalent to 1.8% of strain, is applied using constant displacement on one side and zero displacement (symmetry) on the other. A single node from the latter is pinned to avoid rigid body motion. The rest of the boundaries are left free.

#### 2.4.2 Voids representation

The presence of voids in the laminate is modeled by introducing “weak volumes”, which represent zones where the material behavior is influenced by the presence of a void. The material outside of the weak volume is referred to as “pristine” material. The size of the weak volume,  $100\ \mu\text{m} \times 70\ \mu\text{m} \times 1000\ \mu\text{m}$  (*Z* × *Y* × *X*), corresponds to the size of the *D-region* used for calculation of the effective properties in the micro-model

(Section 2.3.5), and weak volume properties correspond to the effective properties of that region. A weak volume then includes a virtual ellipsoidal void, as illustrated schematically in Fig. 5, and includes a row of five meso-elements in an enriched region (in the X direction) and two adjacent rows of five meso-elements in a non-enriched region (in the Z direction). The size of the void does not affect directly the weak volume size, but has an influence on its material properties as further discussed in Section 2.4.3. For a given void content in the 90° ply, the lower bound for the number of the weak volumes can be calculated by dividing the target void volume by the volume of the virtual void in the weak volume. It is the lower bound because weak volumes are truncated if they cross the ply boundaries.

The weak volumes are distributed within the transverse ply of all meso-models except *Meso-Ref*. The location of a weak volume is determined by its centroid. A distribution algorithm randomizes the location of a new weak volume using uniform probability distribution in all three directions. Overlapping of the new volume with previously positioned ones is not allowed. This process repeats until the desired void content (1.6% or 5%) is reached. The number of weak volumes distributed in the *Meso-S-Low%* and *Meso-S-High%* models is 2878 and 9023 and in the *Meso-L-Low%* and *Meso-L-High%* is 718 and 2246, respectively. In all the models, about half of the distributed weak volumes appear in the enriched regions. Having all the weak volumes in the enriched regions asks for enrichment of the entire transverse ply, which is not possible in the current XFEM implementation in *Abaqus 2017*. The distribution of weak volumes in each model is represented in Fig. 4 c-f. One can notice longer weak volumes in Fig. 6-4d, which are a result of agglomeration of the normal-size weak volumes. This is further discussed in Section 3.2.

#### 2.4.3 Material properties

The material within weak and pristine volumes outside the enriched regions is assumed to be elastic, while inside them it follows a bilinear cohesive law. The latter governs the damage behavior in the enriched elements and requires knowledge of the peak stress (interpreted as transverse strength) for activation of damage, and the area under the traction-separation curve (interpreted as intra-laminar Mode I fracture toughness) for damage evolution. Both elastic and damage related properties for these different regions are extracted from micro-scale models (as discussed in Section 2.3.5 and shown in Fig. 3). Only the in-plane shear modulus ( $G_{LT}$ ) is calculated using analytical formulas of Chamis [38]. The extracted properties from the micro-models are reported in Table 1.

More specifically, elastic properties of the reference material *Meso-Ref* are taken from region *E-Ref-S*. In the models with voids, the transverse stiffness of the entire middle ply (both in weak and pristine volumes) is

1 reduced, while other elastic constants are kept the same as those taken from *E-Ref-S*. The reduced transverse  
2 stiffness is obtained from the micro-scale models with the corresponding void content: homogenization in  
3 regions *E-(S/L)-(Low/High)%* results in the transverse stiffness for *Meso-(S/L)-(Low/High)%*, respectively.  
4 Properties of the 0° plies are left without change, i.e. taken from *E-Ref-S*. The initial stiffness of the bilinear  
5 cohesive law is automatically assigned by the software based on the stiffness of the material in enriched  
6 regions.  
7  
8  
9

10 The transverse strength is obtained as the maximum stress in the effective stress-strain curve for a certain  
11 region (Fig. 3c and f). More specifically, the strength to be used in pristine elements is obtained from *D-Ref-S*  
12 region. The strength in weak elements is obtained from *D-S* region for *Meso-S-(Low/High)%* and from *D-L*  
13 region for *Meso-L-(Low/High)%*. The strength values are reported in Table 1. The void content for analysis of  
14 the transverse stiffness is calculated at the element-level (in the micro-models) and the effect is applied at the  
15 ply-level, while void content for analysis of the strength is analyzed at the ply-level (in the meso-models) and  
16 the effect is applied at the element-level.  
17  
18  
19  
20  
21  
22  
23  
24

25 The fracture toughness is found by fitting the area under the effective stress-strain curve obtained in the  
26 micro-scale model for a specific region to the results of an XFEM single-element model. More specifically, the  
27 effective stress-strain curve for the region *D-Ref-S* is used to get the toughness in pristine elements, while the  
28 fracture toughness in weak elements is obtained from *D-S* region for *Meso-S-(Low/High)%*, and from *D-L* for  
29 *Meso-L-(Low/High)%*. This identification of the fracture toughness via the XFEM single-element modeling  
30 yields a value of 33 J/m<sup>2</sup> for the pristine material, 18 J/m<sup>2</sup> for the weak material with the small void, and 9 J/m<sup>2</sup>  
31 for the one with the large void.  
32  
33  
34  
35  
36  
37  
38

39 There is a variation in local strength and toughness properties of a ply due to microstructural heterogeneity  
40 like fiber distribution. In order to account for the local variation, a random coefficient is taken from a normal  
41 distribution around 1 with the standard deviation of 15% (according to [41]), and is assigned to each enriched  
42 region. The strength of both weak and pristine elements in each enriched region is then modified by  
43 multiplying it by the random coefficient. The fracture toughness of the elements in each enriched region is  
44 multiplied by the square of the coefficient of that region, as proposed in [25].  
45  
46  
47  
48  
49  
50

#### 51 2.4.4 Post-processing: determining the crack density

52 The outcome of the meso-scale modeling is the predicted crack density evolution in function of the applied  
53 strain. In the XFEM, damage occurs on “cohesive surfaces” across the enriched-region elements (Fig. 4g), and  
54 the damage progression is expressed by a status variable, called cohesive scalar damage variable (CSDMG). It  
55  
56  
57  
58  
59  
60  
61  
62  
63  
64  
65

1 is 0 for cohesive surfaces before or at the initiation stage, and reaches 1 for the fully-developed damage, which  
2 corresponds to a traction-free state of the cohesive surface in the element and is interpreted as a physical crack.  
3 Together with the traction-free cohesive surfaces in the neighboring elements a continuous surface can form,  
4 which is referred to as a “traction-free crack”. In [25], the reader can find a detailed discussion on  
5 identification of cracks in XFEM calculations. The predicted crack density at progressive simulation stages is  
6 calculated based on the traction free cracks. For the sake of brevity, they are referred to simply as “cracks”  
7 hereafter. The position, direction, and length of each of the cracks is defined at every step of the simulation, as  
8 illustrated in Fig. 4g.

9  
10  
11 *It is assumed in the software that the crack surface is normal* to the loading direction (global  $0^\circ$ ) since the  
12 normal traction on this surface is at its maximum in comparison to any other possible crack surfaces. *This is a*  
13 *valid assumption especially for rather thick plies such as that being modeled in the current study.*

14  
15  
16  
17  
18  
19  
20  
21 The crack density in calculations can be determined based on two methods. The first method (called here  
22 “Half-Span Method”) counts the number of “well-developed” cracks, while just initiated short cracks are not  
23 counted. In experiments (for example in [42]), it is common to count well-developed cracks, protruding  
24 through more than half of the width of the specimen. Therefore, the crack density is determined as the number  
25 of cracks, which are longer than half of the specimen width, divided by the specimen length. The shorter  
26 cracks are then ignored in this counting method. With the presence of voids, this method neglects the initiation  
27 of cracks originated on one side from a void inside the  $90^\circ$  ply, connecting to the nearest ply boundary, and  
28 counts the crack only when it propagates from the other side of the void to the mid-width of the specimen.  
29 Hence, the effect of voids on the cracking initiation and development would be underestimated.

30  
31  
32  
33  
34  
35  
36  
37  
38  
39  
40  
41  
42  
43  
44  
45  
46  
47  
48  
49  
50  
51  
52  
53  
54  
55  
56  
57  
58  
59  
60  
61  
62  
63  
64  
65  
66  
67  
68  
69  
70  
71  
72  
73  
74  
75  
76  
77  
78  
79  
80  
81  
82  
83  
84  
85  
86  
87  
88  
89  
90  
91  
92  
93  
94  
95  
96  
97  
98  
99  
100  
101  
102  
103  
104  
105  
106  
107  
108  
109  
110  
111  
112  
113  
114  
115  
116  
117  
118  
119  
120  
121  
122  
123  
124  
125  
126  
127  
128  
129  
130  
131  
132  
133  
134  
135  
136  
137  
138  
139  
140  
141  
142  
143  
144  
145  
146  
147  
148  
149  
150  
151  
152  
153  
154  
155  
156  
157  
158  
159  
160  
161  
162  
163  
164  
165  
166  
167  
168  
169  
170  
171  
172  
173  
174  
175  
176  
177  
178  
179  
180  
181  
182  
183  
184  
185  
186  
187  
188  
189  
190  
191  
192  
193  
194  
195  
196  
197  
198  
199  
200  
201  
202  
203  
204  
205  
206  
207  
208  
209  
210  
211  
212  
213  
214  
215  
216  
217  
218  
219  
220  
221  
222  
223  
224  
225  
226  
227  
228  
229  
230  
231  
232  
233  
234  
235  
236  
237  
238  
239  
240  
241  
242  
243  
244  
245  
246  
247  
248  
249  
250  
251  
252  
253  
254  
255  
256  
257  
258  
259  
260  
261  
262  
263  
264  
265  
266  
267  
268  
269  
270  
271  
272  
273  
274  
275  
276  
277  
278  
279  
280  
281  
282  
283  
284  
285  
286  
287  
288  
289  
290  
291  
292  
293  
294  
295  
296  
297  
298  
299  
300  
301  
302  
303  
304  
305  
306  
307  
308  
309  
310  
311  
312  
313  
314  
315  
316  
317  
318  
319  
320  
321  
322  
323  
324  
325  
326  
327  
328  
329  
330  
331  
332  
333  
334  
335  
336  
337  
338  
339  
340  
341  
342  
343  
344  
345  
346  
347  
348  
349  
350  
351  
352  
353  
354  
355  
356  
357  
358  
359  
360  
361  
362  
363  
364  
365  
366  
367  
368  
369  
370  
371  
372  
373  
374  
375  
376  
377  
378  
379  
380  
381  
382  
383  
384  
385  
386  
387  
388  
389  
390  
391  
392  
393  
394  
395  
396  
397  
398  
399  
400  
401  
402  
403  
404  
405  
406  
407  
408  
409  
410  
411  
412  
413  
414  
415  
416  
417  
418  
419  
420  
421  
422  
423  
424  
425  
426  
427  
428  
429  
430  
431  
432  
433  
434  
435  
436  
437  
438  
439  
440  
441  
442  
443  
444  
445  
446  
447  
448  
449  
450  
451  
452  
453  
454  
455  
456  
457  
458  
459  
460  
461  
462  
463  
464  
465  
466  
467  
468  
469  
470  
471  
472  
473  
474  
475  
476  
477  
478  
479  
480  
481  
482  
483  
484  
485  
486  
487  
488  
489  
490  
491  
492  
493  
494  
495  
496  
497  
498  
499  
500  
501  
502  
503  
504  
505  
506  
507  
508  
509  
510  
511  
512  
513  
514  
515  
516  
517  
518  
519  
520  
521  
522  
523  
524  
525  
526  
527  
528  
529  
530  
531  
532  
533  
534  
535  
536  
537  
538  
539  
540  
541  
542  
543  
544  
545  
546  
547  
548  
549  
550  
551  
552  
553  
554  
555  
556  
557  
558  
559  
560  
561  
562  
563  
564  
565  
566  
567  
568  
569  
570  
571  
572  
573  
574  
575  
576  
577  
578  
579  
580  
581  
582  
583  
584  
585  
586  
587  
588  
589  
590  
591  
592  
593  
594  
595  
596  
597  
598  
599  
600  
601  
602  
603  
604  
605  
606  
607  
608  
609  
610  
611  
612  
613  
614  
615  
616  
617  
618  
619  
620  
621  
622  
623  
624  
625  
626  
627  
628  
629  
630  
631  
632  
633  
634  
635  
636  
637  
638  
639  
640  
641  
642  
643  
644  
645  
646  
647  
648  
649  
650  
651  
652  
653  
654  
655  
656  
657  
658  
659  
660  
661  
662  
663  
664  
665  
666  
667  
668  
669  
670  
671  
672  
673  
674  
675  
676  
677  
678  
679  
680  
681  
682  
683  
684  
685  
686  
687  
688  
689  
690  
691  
692  
693  
694  
695  
696  
697  
698  
699  
700  
701  
702  
703  
704  
705  
706  
707  
708  
709  
710  
711  
712  
713  
714  
715  
716  
717  
718  
719  
720  
721  
722  
723  
724  
725  
726  
727  
728  
729  
730  
731  
732  
733  
734  
735  
736  
737  
738  
739  
740  
741  
742  
743  
744  
745  
746  
747  
748  
749  
750  
751  
752  
753  
754  
755  
756  
757  
758  
759  
760  
761  
762  
763  
764  
765  
766  
767  
768  
769  
770  
771  
772  
773  
774  
775  
776  
777  
778  
779  
780  
781  
782  
783  
784  
785  
786  
787  
788  
789  
790  
791  
792  
793  
794  
795  
796  
797  
798  
799  
800  
801  
802  
803  
804  
805  
806  
807  
808  
809  
810  
811  
812  
813  
814  
815  
816  
817  
818  
819  
820  
821  
822  
823  
824  
825  
826  
827  
828  
829  
830  
831  
832  
833  
834  
835  
836  
837  
838  
839  
840  
841  
842  
843  
844  
845  
846  
847  
848  
849  
850  
851  
852  
853  
854  
855  
856  
857  
858  
859  
860  
861  
862  
863  
864  
865  
866  
867  
868  
869  
870  
871  
872  
873  
874  
875  
876  
877  
878  
879  
880  
881  
882  
883  
884  
885  
886  
887  
888  
889  
890  
891  
892  
893  
894  
895  
896  
897  
898  
899  
900  
901  
902  
903  
904  
905  
906  
907  
908  
909  
910  
911  
912  
913  
914  
915  
916  
917  
918  
919  
920  
921  
922  
923  
924  
925  
926  
927  
928  
929  
930  
931  
932  
933  
934  
935  
936  
937  
938  
939  
940  
941  
942  
943  
944  
945  
946  
947  
948  
949  
950  
951  
952  
953  
954  
955  
956  
957  
958  
959  
960  
961  
962  
963  
964  
965  
966  
967  
968  
969  
970  
971  
972  
973  
974  
975  
976  
977  
978  
979  
980  
981  
982  
983  
984  
985  
986  
987  
988  
989  
990  
991  
992  
993  
994  
995  
996  
997  
998  
999  
1000

### 3 Results and discussion

#### 3.1 Effect of voids on properties at the micro-scale

The elastic constants obtained from elastic homogenization of the four micro-scale models are presented in Table 1. Volumes with different sizes are chosen in the RVEs and RDVs (as indicated in Fig. 3). This allows studying the local effect of the voids on elastic constants as well as calculating effective degraded properties to be fed into the weak volumes of the meso-scale models. According to the results in Table 1, there are two parameters affecting the elastic constants: the fiber volume fraction and void content. The highest sensitivity is

noted for transverse elastic moduli and out-of-plane shear moduli, while longitudinal elastic moduli and Poisson's ratios are negligibly sensitive to the void content, but dependent on the fiber volume fraction.

The micro-scale models show that voids initiate transverse cracks as shown in Fig. 3b and e, and the transverse strength and the strain to failure are reduced in the presence of voids (Fig. 3c and f). For the same void content, the reduction caused by the larger void is higher. Moreover, the influence of void content on transverse strength is less significant than that of void size. The abrupt drops in the effective stress-strain curves correspond to the full volume of the micro-models, where a sudden crack leads to the total loss of the load carrying ability of the modeled material. For the smaller regions, the curves do not show abrupt drops. This is because the crack opening is more significant when compared to the length of the smaller regions and therefore causes a significant increase in strain. In the full volume of the micro-models, the crack opening is negligible compared to the length of the region, causing negligible increase in strain.

Although the homogenized elastic constants obtained from either of the reference micro-models, i.e. *Micro-Ref-S* and *Micro-Ref-L*, are sufficient as input for the pristine material in the meso-scale models, the homogenization results of both models are reported (in Table 1) to show the small statistical variation caused by the variation in the fiber distribution. Moreover, having a reference model for each void-size case allows qualitative comparison of crack initiation and propagation in the absence and presence of the voids.

### 3.2 Effect of voids on transverse cracking

Fig. 6 shows the crack density predictions in all meso-models, using the Half-Span Method (Fig. 6a) and Surface Area Method (Fig. 6b). The results of both methods are close to each other and show the same trend. The Surface Area Method produces smoother growth of the crack density with the applied load. As explained in Section 2.4.4, it considers all cracks regardless of their length and hence provides a more precise analysis of crack density. It is used in the discussion below.

The crack density vs. applied strain curves (Fig. 6b) demonstrate that the presence of voids influences the cracking onset threshold and the crack density at the progressive stages of the loading. Comparing the two extreme cases, the reference case and the case with 5% of small voids (having the largest number of voids), it is seen that the onset of the steady progressive cracking (indicated with an arrow in Fig. 6b and explained below) is shifted from ~0.6% in the reference model down to ~0.5% in the model with voids. The crack density during the loading is consistently (about 0.3 to 1.0 cracks/mm) higher in the model with voids; for instance, the difference at 0.6% applied strain is ~0.75 cracks/mm, at 0.9% is ~0.5 cracks/mm, and at 1.2% is



1 ~0.6 cracks/mm. The maximum crack density in both cases is ~5 cracks/mm, which is due to a limitation of  
2 the model (as explained in the end of the section).

3 The cracking onset can be defined in two ways: the appearance of the very first crack and the onset of the  
4 steady progressive cracking. The first type is predicted to happen at 0.5% applied strain in the reference case.  
5 Presence of voids, regardless of their content percentage or their size, reduces the “strain at first crack” to  
6 0.2%...0.4%, as tabulated in Fig 5b. Early stages of loading in meso-scale models are illustrated in Fig. 7,  
7 where cracks are initiated mainly from weak volumes. Further on cracks propagate rapidly through the  
8 specimen’s width. The finding that voids influence the initial stages of cracking is consistent with experimental  
9 observations, e.g. in [15-17]. The strain at first crack can be expected to depend strongly on the particular  
10 instance of the stochastic realization of the void position and of the strength distribution in the 90° ply. Thus,  
11 analysis of the strain at first crack for different variants of the voids, as simulated and presented in Fig. 6b,  
12 should be performed with caution. However, the lowest strain at first crack of 0.2% for *Meso-L-High%* and  
13 0.3% for *Meso-L-Low%* (two cases with large voids) can also have a physical explanation: large voids with a  
14 transversal axes mean of 60 μm, or about 1/3 of the ply thickness, create larger stress concentrations leading to  
15 a crack across the ply, than smaller 30-μm voids.  
16  
17  
18  
19  
20  
21  
22  
23  
24  
25  
26  
27  
28

29 The second definition of cracking onset is the start of steady progressive cracking, which appears as a knee  
30 in the crack density vs. applied strain curve (indicated with an arrow in Fig. 6b). In the current calculations, the  
31 knee point is the first data point, where one of the following statements holds true: a) at least, three new cracks  
32 are developed, i.e. the crack density is increased by a value  $\geq 0.15$  cracks/mm, or (b) at least, three consecutive  
33 points with minimum one new crack development occur, i.e. the crack density is increased at each of the  
34 consecutive points by a value  $\geq 0.05$  cracks/mm. This definition of cracking onset is expected to give a more  
35 stable characteristic of the crack density evolution due to lower sensitivity to the stochastic variability of the  
36 void positioning and local strength in the ply.  
37  
38  
39  
40  
41  
42  
43  
44  
45

46 The simulation results show that the onset of steady cracking shifts to lower strains only if the number of  
47 voids is sufficiently large. The strain to onset of steady cracking for *Meso-S-Low%*, *Meso-L-Low%*, and *Meso-*  
48 *L-high%* is respectively 0.65%, 0.66%, 0.61% which is close to that for the reference case, i.e. 0.63%.  
49

50 However, *Meso-S-High%* shows a lower strain to onset of steady cracking, namely 0.50%. A high volume  
51 fraction of small voids (in *Meso-S-High%*) results in a larger number of voids, compared to the other cases  
52 (Fig. 4c-f). Larger number of voids results in their closer positioning, which can lead to void agglomeration.  
53 The agglomeration level can be defined as the number of touching weak volumes (with no elements in  
54  
55  
56  
57  
58  
59  
60  
61  
62  
63  
64  
65

between) within enriched regions divided by the total number of weak volumes. With this definition, the agglomeration level in *Meso-L-Low%* and *Meso-L-High%* is 29% and 64%, respectively, and in *Meso-S-Low%* and *Meso-S-High%* it is 74% and 100%, respectively. In *Meso-S-High%*, all the weak volumes touch each other, which create larger continuous regions with degraded properties, facilitating crack propagation. Physically, this corresponds to cracks connecting the voids.

Once a steady cracking stage is reached, further cracking progresses with almost the same crack density growth rate, meaning that the crack density vs. applied strain curves stay parallel. This may point out that the crack density evolution after the onset of steady cracking is not a void-related phenomenon and is governed by the same relations between the stress redistribution in the ply upon crack formation and the local ply strength. The maximum crack density predicted in all the models converges to ~5 cracks/mm, which is the limitation of the model. As stated in Section 2.4, the number of enriched regions in the model is limited to 100 by *Abaqus 2017*. Considering the length of the model (20 mm), this means that the crack density cannot exceed 5 cracks/mm. To correctly predict the crack density at saturation, one would need to increase the number of enriched regions in the model.

A multi-scale experimental study on the effect of voids on the evolution of transverse cracking was performed in [18], where voidy carbon/epoxy cross-ply laminates were produced with the same cure conditions as that mentioned in Section 2.2. It was found that the chosen cure parameters led to not only the voids but also an incomplete cure of the matrix. The meso-scale measurements revealed that the combination of the voids and incomplete matrix cure is responsible for a dramatic decrease of the strain to onset cracking and an increase of the crack density at saturation, both measured at the laminate's edge. The micro-scale analysis showed clear evidence for voids triggering the first cracks. Although results of this experimental investigation agree in general with those of the current study, there are some barriers for a quantitative comparison of the results. These are as follows: 1) the constituents' properties in the micro-model do not necessarily correspond to the experimentally tested material; 2) in the experiments, there is another factor influencing the cracking in addition to the voids, namely incomplete matrix cure, which is not accounted for in the modeling; 3) the voids' characteristics are not the same in the modeling and the experiments, and are difficult to be controlled in the latter; 4) the laminate stacking sequence is different in the modeled and tested materials; 5) the crack density in the modeling is calculated using cracks' surfaces in 3D, while in the experiments, it is measured only at the laminate's edge; and 6) the modeling approach has limitations in

prediction of the crack density at saturation. Once these issues are resolved, one should be able to compare and validate the predictions against the experimental results.

#### 4 Concluding remarks

We have developed and presented in this paper a combined two-scale methodology for simulation of the matrix cracking in cross-ply composite laminates in the presence of voids. The micro-scale model simulates matrix cracking in a “representative defective volume” with direct representation of a random placement of unidirectional fibers around a void. The meso-scale model simulates cracking in the 90° ply of a cross-ply laminate, utilizing XFEM. The effective properties of the material at the micro-scale are used as input parameters for the meso-scale model, including weak volumes in the 90° ply, representing the material degraded by voids. The key feature of the model is a link between the micro- and meso-scales. A scale link between the micro- and meso-model is created, which adequately accounts for the influence of the micro-scale model size on its effective mechanical behavior.

Application of the two-scale modeling methodology to cracking evolution under tension loading is explored in a typical [0°/90°/0°] carbon fiber-reinforced epoxy laminate in the presence of voids for two levels of the void content (1.6% and 5%) and two levels of the void size (30- $\mu\text{m}$  and 60- $\mu\text{m}$  diameter). The characteristic features of the cracking evolution with increase of the applied tensile strain are as follows:

1. The maximum effect of the presence of voids is observed in the model with 30- $\mu\text{m}$  voids and 5% void content. The onset of the steady progressive cracking is shifted down to ~0.5% from ~0.6% in the reference model. The crack density during the loading is consistently higher in the presence of voids, with a difference of ~20% in the middle of the loading, i.e. ~0.9% applied strain.
2. The presence of voids affects the strain corresponding to initiation of the first crack, decreasing the strain at first crack from 0.5% in the reference model down to 0.2%-0.4% in the presence of voids (depending on the voids' parameters).
3. The onset of the steady cracking (a knee on the crack density vs. applied strain curve) changes significantly only for the case of high (5%) void content and smaller (30  $\mu\text{m}$ ) voids size, i.e. *Meso-S-High%*. For other cases, the voids do not affect this threshold. This difference in behavior is attributed to a much higher number of voids in *Meso-S-High%* case, causing higher degree of voids' agglomeration.
4. The growth rate of the crack density vs. applied strain curves does not change with the presence of voids.

Generalizing these features, the present simulations suggest that the presence of voids:

- affects the onset and development of first sporadic cracks, associated with voids;
- affects the onset of the steady progressive cracking only if the void content is sufficiently high and the voids are placed with sufficient density;
- does not affect the rate of cracking.

Simulation of matrix cracking in the presence of voids allows analyses which are not always feasible to perform experimentally. For instance, it allows 1) identifying the effect of voids without a need of (a large number of) experimental tests that are typically costly and eco-unfriendly, 2) performing parametric studies on the effects of voids' characteristics, such as size and morphology, on cracking, which is not achievable experimentally, and 3) 3D analysis of the interaction between voids and cracks, which is also possible using *in-situ* micro-CT, but only on small samples that may not be representative. Furthermore, the developed methodology is useful for simulation of matrix cracking in other laminate configurations as well as other types of defects.

Although promising, the developed methodology needs further work. For example, prediction of crack densities at saturation requires enhancement of the XFEM technique, particularly on the side of the enrichments. Delamination, being another important damage mechanism in composites, should be included in the analysis. For higher accuracy of predictions, one should also account for the residual thermal stresses.

### Acknowledgments

The authors gratefully acknowledge *SIM* (Strategic Initiative Materials in Flanders) and *VLAIO* (Flemish government agency for Innovation and Entrepreneurship) for their support of the *IBO* project *M3Strength*, which is part of the research program *MacroModelMat (M3)*, coordinated by Siemens (Siemens PLM Software, Belgium). The micro-scale modeling was performed in the framework of the *M3Strength* project. They also would like to acknowledge support of Skolkovo Institute of Science and Technology through the 335-MRA project, in the framework of which the meso-scale modeling was performed. The authors are grateful to K. Verjans and S. Wathiong for their help in production of composite laminates at SABCA Limburg NV, Belgium. The micro-CT imaging was performed at Inside Matters NV, Belgium. S.V. Lomov holds Toray Chair for Composite Materials at KU Leuven.

### References

1. Mehdikhani, M., L. Gorbatikh, I. Verpoest, and S.V. Lomov, Voids in fiber-reinforced polymer composites: a review on their formation, characteristics, and effects on mechanical performance. *Journal of Composite Materials*, 2018: p. In print.
2. Judd, N.C.W. and W.W. Wright, Voids and Their Effects on the Mechanical Properties of Composites - An Appraisal. *Sampe Journal*, 1978. 14(1): p. 10-14.
3. Talreja, R., 5 - Manufacturing defects in composites and their effects on performance, in *Polymer Composites in the Aerospace Industry*. 2015, Woodhead Publishing. p. 99-113.
4. Olivier, P., J.P. Cottu, and B. Ferret, Effects of cure cycle pressure and voids on some mechanical properties of carbon/epoxy laminates. *Composites*, 1995. 26(7): p. 509-515.
5. Huang, H. and R. Talreja, Effects of void geometry on elastic properties of unidirectional fiber reinforced composites. *Composites Science and Technology*, 2005. 65(13): p. 1964-1981.
6. de Almeida, S.F.M. and Z.d.S.N. Neto, Effect of void content on the strength of composite laminates. *Composite Structures*, 1994. 28(2): p. 139-148.
7. Lambert, J., A.R. Chambers, I. Sinclair, and S.M. Spearing, 3D damage characterisation and the role of voids in the fatigue of wind turbine blade materials. *Composites Science and Technology*, 2012. 72(2): p. 337-343.
8. Seon, G., A. Makeev, Y. Nikishkov, and E. Lee, Effects of defects on interlaminar tensile fatigue behavior of carbon/epoxy composites. *Composites Science and Technology*, 2013. 89: p. 194-201.
9. Carraro, P.A., L. Maragoni, and M. Quaresimin, Influence of manufacturing induced defects on damage initiation and propagation in carbon/epoxy NCF laminates. *Advanced Manufacturing: Polymer & Composites Science*, 2015. 1(1): p. 44-53.
10. Maragoni, L., P.A. Carraro, M. Peron, and M. Quaresimin, Fatigue behaviour of glass/epoxy laminates in the presence of voids. *International Journal of Fatigue*, 2017. 95: p. 18-28.
11. Ashouri Vajari, D., C. González, J. Llorca, and B.N. Legarth, A numerical study of the influence of microvoids in the transverse mechanical response of unidirectional composites. *Composites Science and Technology*, 2014. 97: p. 46-54.
12. Aratama, S., R. Hashizume, K. Takenaka, K. Koga, Y. Tsumura, T. Miyake, M. Nishikawa, and M. Hojo, Microscopic observation of voids and transverse crack initiation in CFRP laminates. *Advanced Composite Materials*, 2016. 25(sup1): p. 115-130.

13. Mehdikhani, M., M. Aravand, B. Sabuncuoglu, M.G. Callens, S.V. Lomov, and L. Gorbatikh, Full-field strain measurements at the micro-scale in fiber-reinforced composites using digital image correlation. *Composite Structures*, 2016. 140: p. 192-201.
14. Nairn, J.A., Matrix microcracking in composites. *Polymer matrix composites*, 2000. 2: p. 403-432.
15. Talreja, R., Studies on the failure analysis of composite materials with manufacturing defects. *Mechanics of Composite Materials*, 2013. 49(1): p. 35-44.
16. Sisodia, S., E.K. Gamstedt, F. Edgren, and J. Varna, Effects of voids on quasi-static and tension fatigue behaviour of carbon-fibre composite laminates. *Journal of Composite Materials*, 2014.
17. Huang, Y., J. Varna, and R. Talreja, Statistical methodology for assessing manufacturing quality related to transverse cracking in cross ply laminates. *Composites Science and Technology*, 2014. 95: p. 100-106.
18. Mehdikhani, M., E. Steensels, A. Standaert, K.A.M. Vallons, L. Gorbatikh, and S.V. Lomov, Multi-scale digital image correlation for detection and quantification of matrix cracks in carbon fiber composite laminates in the absence and presence of voids controlled by the cure cycle. *Composites Part B: Engineering*, 2018. 154: p. 138-147.
19. Herráez, M., D. Mora, F. Naya, C.S. Lopes, C. González, and J. LLorca, Transverse cracking of cross-ply laminates: A computational micromechanics perspective. *Composites Science and Technology*, 2015. 110: p. 196-204.
20. Garoz, D., F.A. Gilabert, R.D.B. Sevenois, S.W.F. Spronk, and W. Van Paepegem, Material parameter identification of the elementary ply damage mesomodel using virtual micro-mechanical tests of a carbon fiber epoxy system. *Composite Structures*, 2017. 181: p. 391-404.
21. LLorca, J., C. González, J.M. Molina- Aldareguía, J. Segurado, R. Seltzer, F. Sket, M. Rodríguez, S. Sádaba, R. Muñoz, and L.P. Canal, Multiscale modeling of composite materials: a roadmap towards virtual testing. *Advanced Materials*, 2011. 23(44): p. 5130-5147.
22. García, I.G., B.J. Carter, A.R. Ingraffea, and V. Mantič, A numerical study of transverse cracking in cross-ply laminates by 3D finite fracture mechanics. *Composites Part B: Engineering*, 2016. 95: p. 475-487.
23. Iarve, E.V., M.R. Gurvich, D.H. Mollenhauer, C.A. Rose, and C.G. Davila, Mesh-independent matrix cracking and delamination modeling in laminated composites. *International Journal for Numerical Methods in Engineering*, 2011. 88(8): p. 749-773.
24. Swindeman, M.J., E.V. Iarve, R.A. Brockman, D.H. Mollenhauer, and S.R. Hallett, Strength Prediction in Open Hole Composite Laminates by Using Discrete Damage Modeling. *Aiaa Journal*, 2013. 51(4): p. 936-945.

- 1  
2  
3  
4  
5  
6  
7  
8  
9  
10  
11  
12  
13  
14  
15  
16  
17  
18  
19  
20  
21  
22  
23  
24  
25  
26  
27  
28  
29  
30  
31  
32  
33  
34  
35  
36  
37  
38  
39  
40  
41  
42  
43  
44  
45  
46  
47  
48  
49  
50  
51  
52  
53  
54  
55  
56  
57  
58  
59  
60  
61  
62  
63  
64  
65
25. Petrov, N.A., L. Gorbatikh, and S.V. Lomov, A parametric study assessing performance of eXtended Finite Element Method in application to the cracking process in cross-ply composite laminates. *Composite Structures*, 2018. 187: p. 489-497.
  26. Melro, A.R., P.P. Camanho, F.M. Andrade Pires, and S.T. Pinho, Micromechanical analysis of polymer composites reinforced by unidirectional fibres: Part I – Constitutive modelling. *International Journal of Solids and Structures*, 2013. 50(11–12): p. 1897-1905.
  27. Melro, A.R., P.P. Camanho, F.M. Andrade Pires, and S.T. Pinho, Micromechanical analysis of polymer composites reinforced by unidirectional fibres: Part II – Micromechanical analyses. *International Journal of Solids and Structures*, 2013. 50(11–12): p. 1906-1915.
  28. Carraro, P.A., L. Maragoni, and M. Quaresimin, Prediction of the crack density evolution in multidirectional laminates under fatigue loadings. *Composites Science and Technology*, 2017. 145: p. 24-39.
  29. Kakakasery, J., V. Arumugam, K. Abdul Rauf, D. Bull, A.R. Chambers, C. Scarponi, and C. Santulli, Cure cycle effect on impact resistance under elevated temperatures in carbon prepreg laminates investigated using acoustic emission. *Composites Part B: Engineering*, 2015. 75: p. 298-306.
  30. Masschaele, B., M. Dierick, D. Van Loo, M.N. Boone, L. Brabant, E. Pauwels, V. Cnudde, and L. Van Hoorebeke. HECTOR: A 240kV micro-CT setup optimized for research. in *Journal of Physics: Conference Series*. 2013. IOP Publishing.
  31. Straumit, I., S.V. Lomov, and M. Wevers, Quantification of the internal structure and automatic generation of voxel models of textile composites from X-ray computed tomography data. *Composites Part A: Applied Science and Manufacturing*, 2015. 69: p. 150-158.
  32. Nguyen, N.Q., M. Mehdikhani, I. Straumit, L. Gorbatikh, L. Lessard, and S.V. Lomov, Micro-CT measurement of fibre misalignment: Application to carbon/epoxy laminates manufactured in autoclave and by vacuum assisted resin transfer moulding. *Composites Part A: Applied Science and Manufacturing*, 2018. 104: p. 14-23.
  33. Melro, A.R., P.P. Camanho, and S.T. Pinho, Generation of random distribution of fibres in long-fibre reinforced composites. *Composites Science and Technology*, 2008. 68(9): p. 2092-2102.
  34. Romanov, V., S.V. Lomov, Y. Swolfs, S. Orlova, L. Gorbatikh, and I. Verpoest, Statistical analysis of real and simulated fibre arrangements in unidirectional composites. *Composites Science and Technology*, 2013. 87: p. 126-134.

- 1  
2  
3  
4  
5  
6  
7  
8  
9  
10  
11  
12  
13  
14  
15  
16  
17  
18  
19  
20  
21  
22  
23  
24  
25  
26  
27  
28  
29  
30  
31  
32  
33  
34  
35  
36  
37  
38  
39
35. Fiedler, B., M. Hojo, S. Ochiai, K. Schulte, and M. Ando, Failure behavior of an epoxy matrix under different kinds of static loading. *Composites Science and Technology*, 2001. 61(11): p. 1615-1624.
  36. Tschoegl, N.W., Failure surfaces in principal stress space. *Journal of Polymer Science Part C: Polymer Symposia*, 1971. 32(1): p. 239-267.
  37. Barbero, E.J., *Finite Element Analysis of Composite Materials*. 2007: Taylor & Francis.
  38. Chamis, C.C., Mechanics of composite materials: past, present, and future. *Journal of Composites, Technology and Research*, 1989. 11(1): p. 3-14.
  39. Vaughan, T.J. and C.T. McCarthy, A combined experimental–numerical approach for generating statistically equivalent fibre distributions for high strength laminated composite materials. *Composites Science and Technology*, 2010. 70(2): p. 291-297.
  40. Maragoni, L., P.A. Carraro, and M. Quaresimin, Development, validation and analysis of an efficient micro-scale representative volume element for unidirectional composites. *Composites Part A: Applied Science and Manufacturing*, 2018. 110: p. 268-283.
  41. van der Meer, F.P. and C.G. Dávila, Cohesive modeling of transverse cracking in laminates under in-plane loading with a single layer of elements per ply. *International Journal of Solids and Structures*, 2013. 50(20): p. 3308-3318.
  42. Yokozeki, T., Y. Iwahori, and S. Ishiwata, Matrix cracking behaviors in carbon fiber/epoxy laminates filled with cup-stacked carbon nanotubes (CSCNTs). *Composites Part A: Applied Science and Manufacturing*, 2007. 38(3): p. 917-924.

#### 40 41 42 43 44 45 46 47 48 49 50 51 52 53

**Figure captions**

41  
42  
43  
44  
45

**Figure 1.** The combined two-scale approach: phenomena and features to be considered in the models – the roadmap for numerical modeling of the effect of voids on matrix cracking.

46  
47  
48  
49  
50  
51  
52  
53

**Figure 2.** Void size characterization using micro-CT: (a) a 3D visualization of voids in the cross-ply [0/90]<sub>4s</sub> carbon fiber/epoxy laminate and definition of the void axes; relative frequency distributions of (b) the geometric mean of the transversal axes, (c) the major axis, (d) the cross-section roundness factor, (e) the elongation factor, and (f) the void in-plane orientation.

54  
55  
56  
57  
58  
59  
60  
61  
62  
63  
64  
65

**Figure 3.** Micro-scale modeling of matrix damage under transverse tension in (a), (b) the small and (d), (e) the large model; (c), (f) their corresponding effective stress-strain curves for different regions that are indicated on the micro-models – due to symmetry, half-width models are considered.



**Figure 4.** Representation of the (a) lay-up and geometry of the meso-scale model, (b) laminate mesh with enriched regions (dark green) in the transverse ply; weak volumes (light green) distributed in the transverse ply of (c) Meso-S-Low%, (d) Meso-S-High%, (e) Meso-L-Low%, and Meso-L-High%; (g) cracks in Meso-S-Low% (as an example) initiated from the weak volumes (at 0.72% of applied strain) – blue represents the regions between the enriched regions in the transverse ply.

**Figure 5.** Schematic representation of a weak volume (a) in enriched regions (occupying five elements) and (b) in non-enriched regions (occupying ten elements) – the blocks show meso-scale elements and the ellipsoid is a virtual void inside the weak volume – the color scheme corresponds to the elements in the enriched and non-enriched regions shown in Fig. 4b.

**Figure 6.** Density of traction-free cracks vs. the applied strain – crack density calculated with (a) Half-Span Method: the number of cracks reached the half of the width divided by the specimen length, (b) Surface Area Method: the total surface area of the cracks divided by the transverse ply volume. The tables present the strain level at both first crack and steady cracking onset for the different models.

**Figure 7.** Crack surfaces as predicted in the meso-models: (a) Meso-S-Low% and (b) Meso-L-Low% both at 0.54% applied strain, (c) Meso-S-High% and (d) Meso-L-High% both at 0.45% of applied strain – CSDMG stands for cohesive scalar damage variable and red color denotes traction-free crack surfaces.

**Table 1** Elastic properties and strength, obtained numerically for different regions, with different fiber volume fraction ( $V_f$ ) and void content ( $V_v$ ), in the four micro-models.

Model without a void									Model with a void							
Region size ( $\mu\text{m}^2$ )	Region ID	Volume fraction (%)	$E_L$ (GPa)	$E_T$ (GPa)	$\nu_{LT}$	$\nu_{TT}$	$G_{TT}$ (GPa)	$\sigma_T$ (MPa)	Region ID	Volume fraction (%)	$E_L$ (GPa)	$E_T$ (GPa)	$\nu_{LT}$	$\nu_{TT}$	$G_{TT}$ (GPa)	$\sigma_T$ (MPa)
<i>Micro-Ref-S</i>									<i>Micro-Void-S</i>							
210 × 105	<i>E-Ref-S</i>	$V_f=57.6$ $V_v=0$	<b>P,W, all</b>	<b>whole Meso-Ref; 0° plies, all models</b>	<b>P,W, all</b>	<b>P,W, all</b>	<b>P,W, all</b>	<b>pristine, all models</b>	<i>E-S-Low%</i>	$V_f=57.2$ $V_v=1.60$	134	<b>90° ply, Meso-S-Low%</b>	0.34	0.52	2.61	48.8
			<b>135</b>	<b>8.04</b>	<b>0.34</b>	<b>0.54</b>	<b>2.61</b>	<b>64.14</b>				<b>7.74</b>				
119 × 119	-	$V_f=59.2$ $V_v=0$	139	8.21	0.34	0.53	2.68	65.1	<i>E-S-High%</i>	$V_f=57.8$ $V_v=5.05$	136	<b>90° ply, Meso-S-High%</b>	0.33	0.52	2.53	47.9
												<b>7.67</b>				
100 × 70	<i>D-Ref-S</i>	$V_f=57.1$ $V_v=0$	135	8.04	0.34	0.54	2.62	64.2	<i>D-S</i>	$V_f=54.3$ $V_v=10.2$	128	6.92	0.34	0.52	2.27	<b>weak, Meso-S-High/Low%</b>
												<b>43.3</b>				
<i>Micro-Ref-L</i>									<i>Micro-Void-L</i>							
420 × 210	-	$V_f=57.9$ $V_v=0$	136	8.03	0.34	0.54	2.61	64.2	<i>E-L-Low%</i>	$V_f=57.1$ $V_v=1.60$	134	<b>90° ply, Meso-L-Low%</b>	0.34	0.53	2.52	36.0
												<b>7.71</b>				
238 × 238	-	$V_f=57.5$ $V_v=0$	136	8.04	0.34	0.54	2.61	64.3	<i>E-S-High%</i>	$V_f=55.1$ $V_v=5.02$	129	<b>90° ply, Meso-L-High%</b>	0.34	0.53	2.44	34.7
												<b>7.45</b>				
100 × 70	-	$V_f=56.0$ $V_v=0$	132	7.73	0.34	0.55	2.49	62.8	<i>D-L</i>	$V_f=35.4$ $V_v=41.0$	83.2	3.44	0.36	0.59	1.08	<b>weak, Meso-L-High/Low%</b>
												<b>16.7</b>				

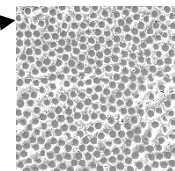
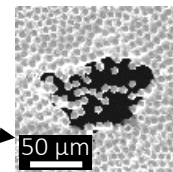
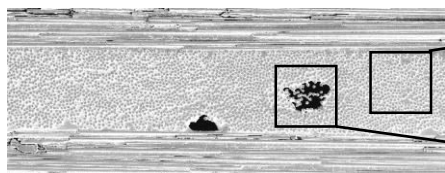
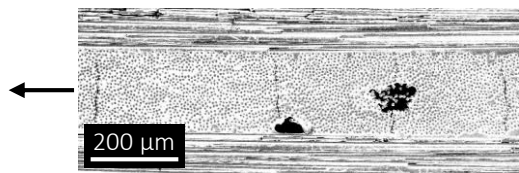
Notes:

1. The **bold** values are used as the input for the meso-models that are specified above them.
2. “**P,W, all**” means “pristine and weak elements, all models”.
3. Regions ID’s are given for regions, of which the properties were transferred to the meso-models and indicated in Fig. 3.

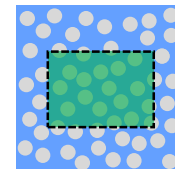
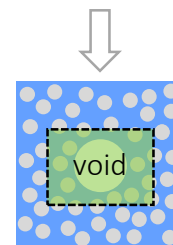
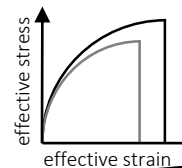
Figure(s)

Matrix cracking

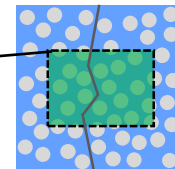
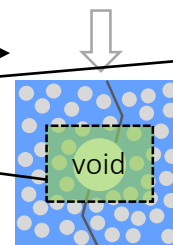
Intra-laminar voids



Step 1: micro-scale finite element model with matrix plasticity and damage  
Step 2: random distribution of weak volumes with effective properties  
Step 3: cracking prediction with extended finite element method



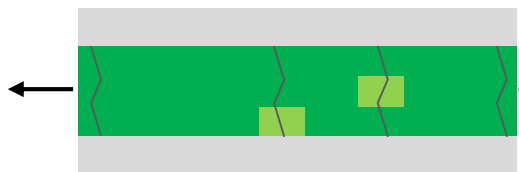
Step 1



Representative volume element

Step 2

Representative defective volume



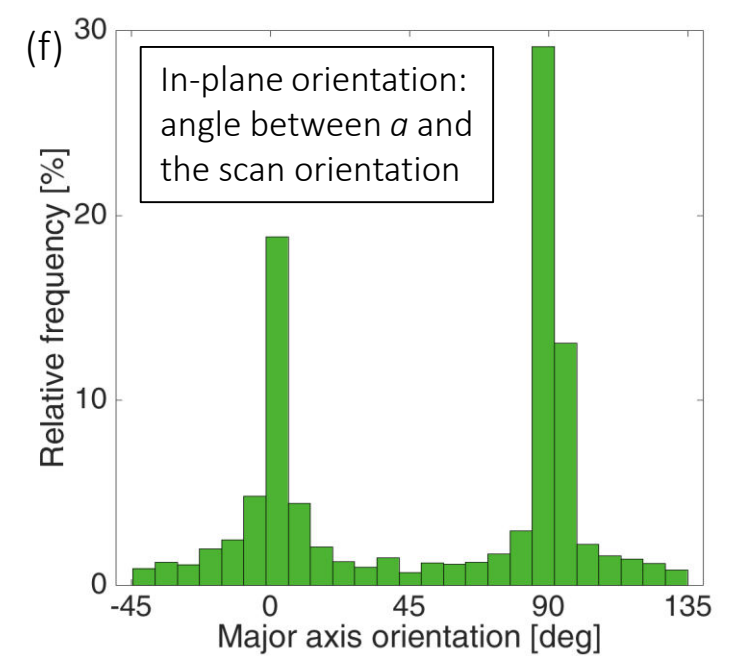
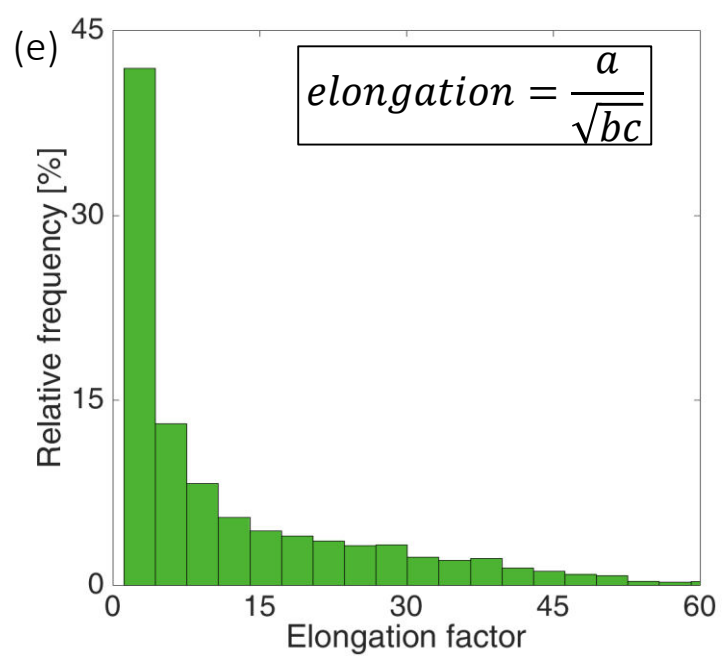
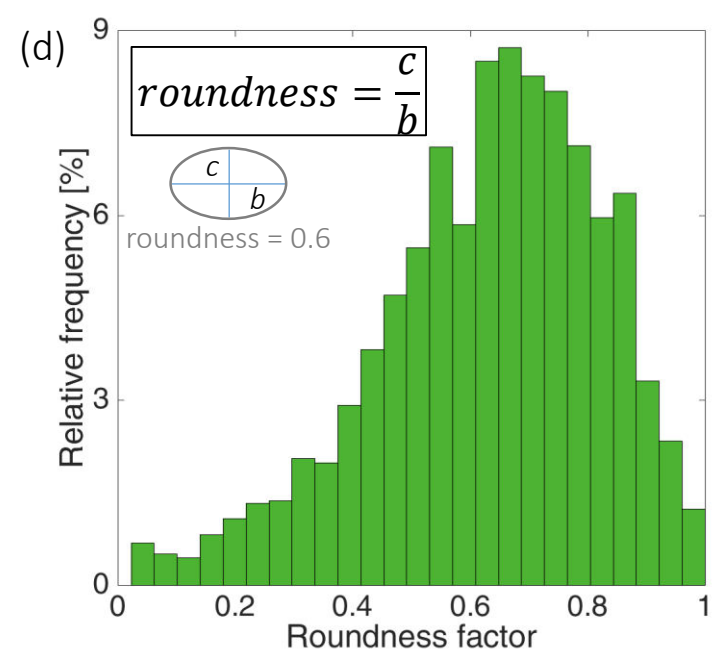
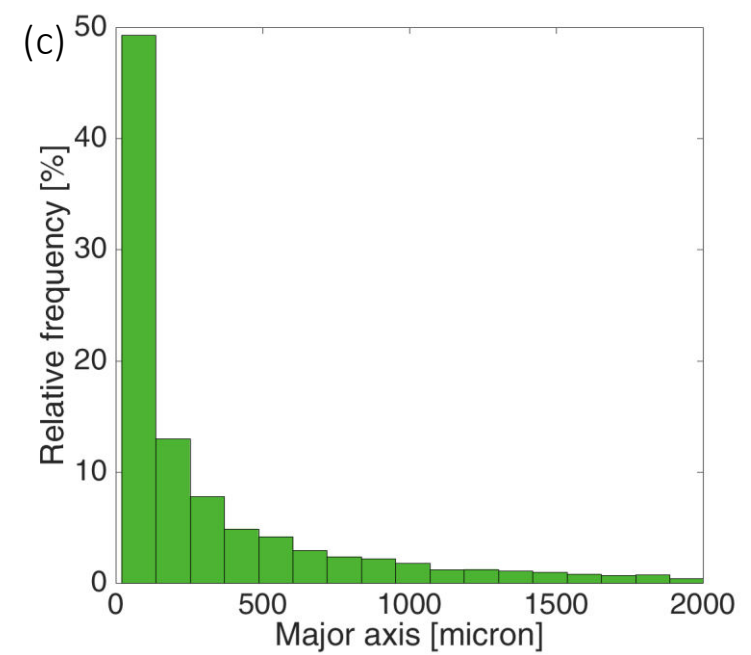
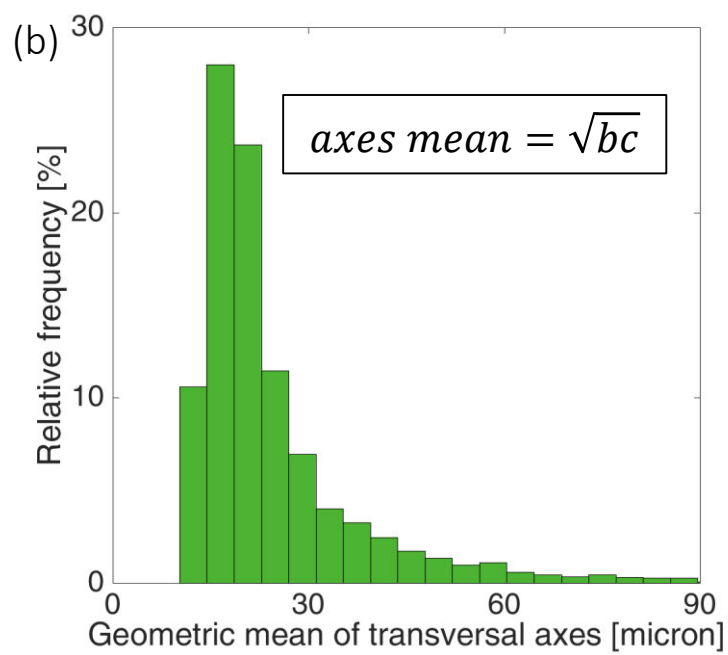
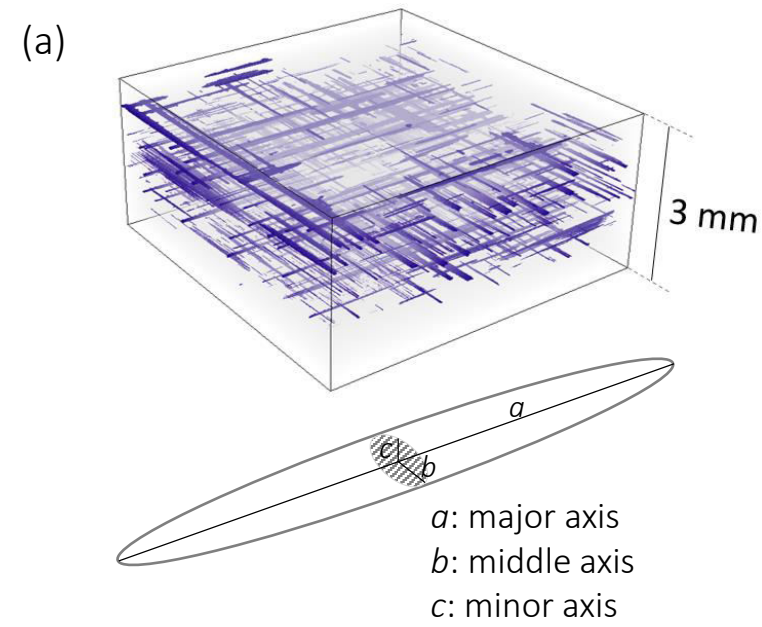
Predicted matrix cracking in transverse plies

Step 3

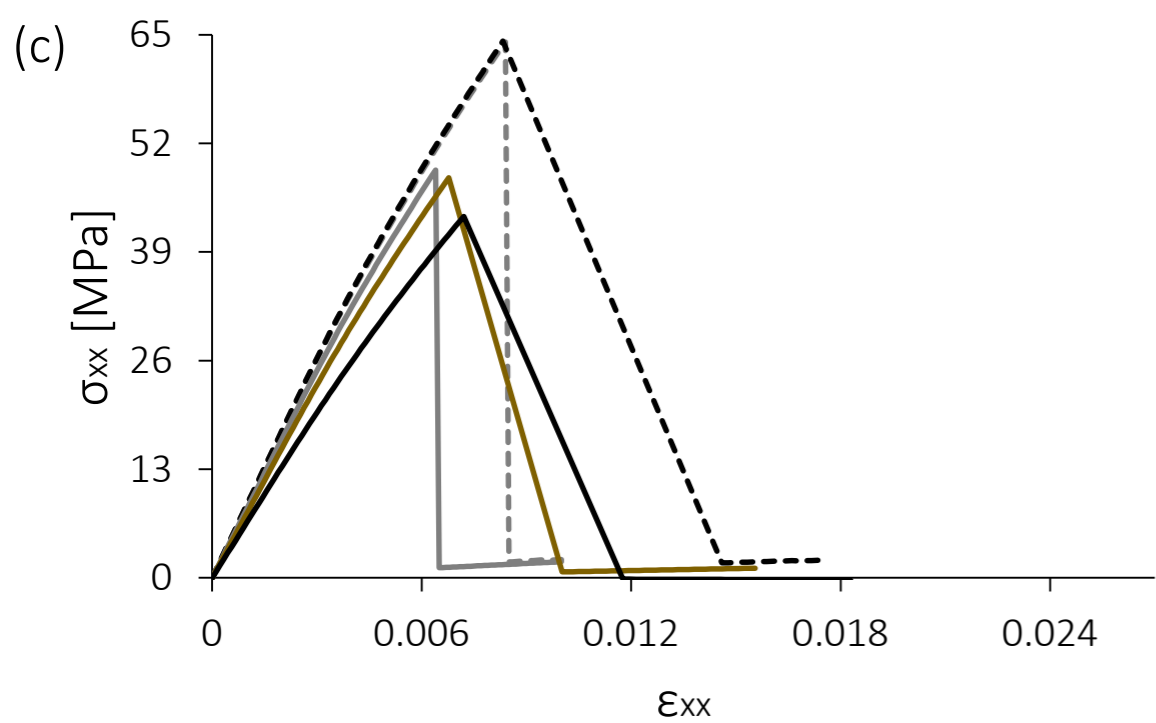
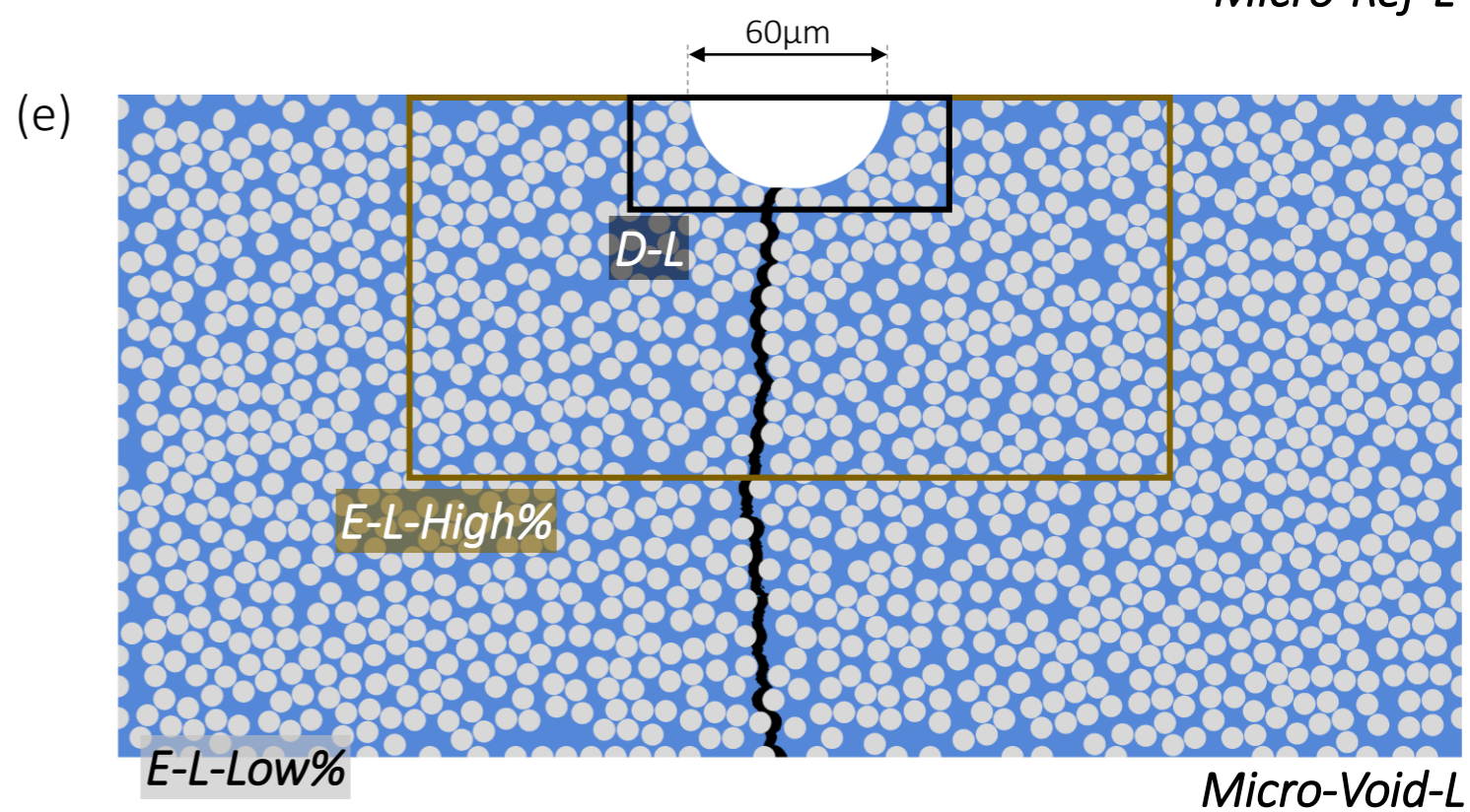
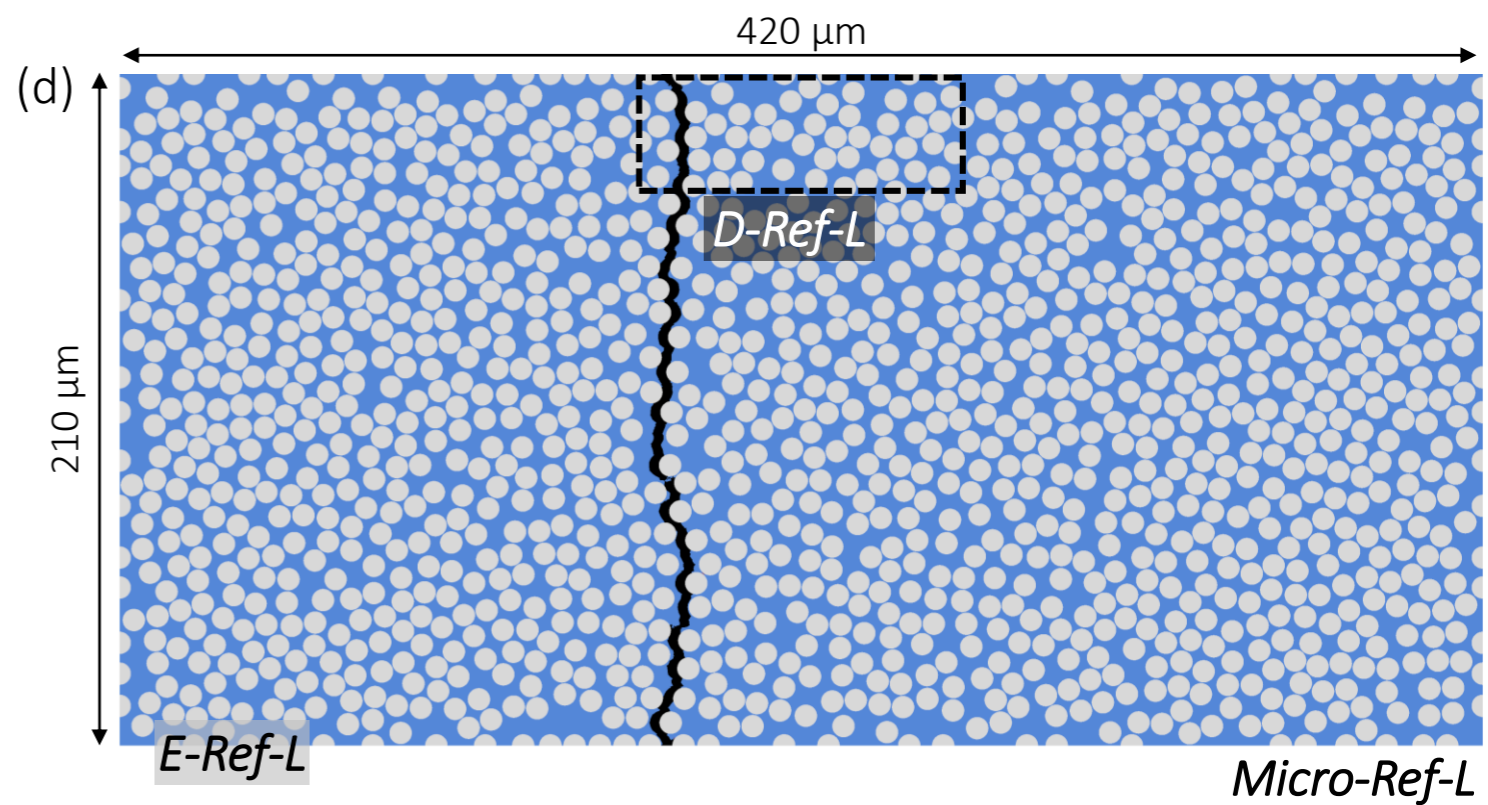
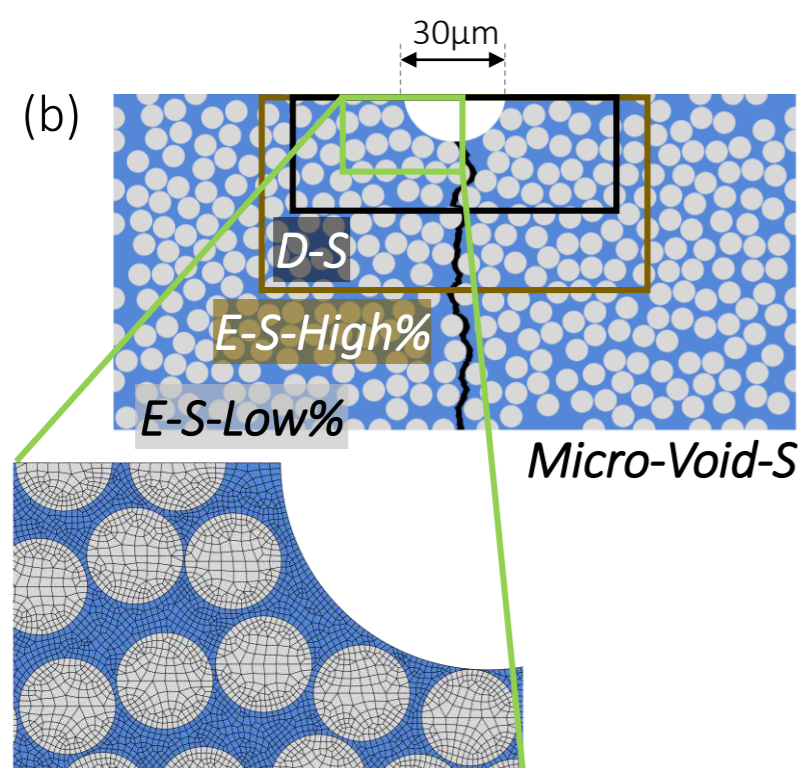
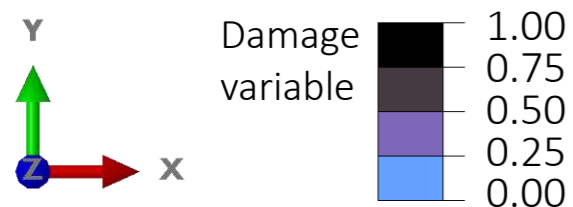
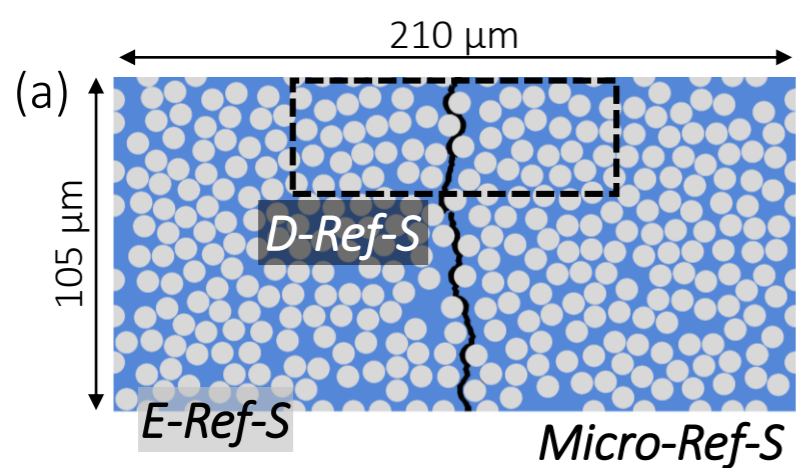


Weak and pristine volumes with effective properties

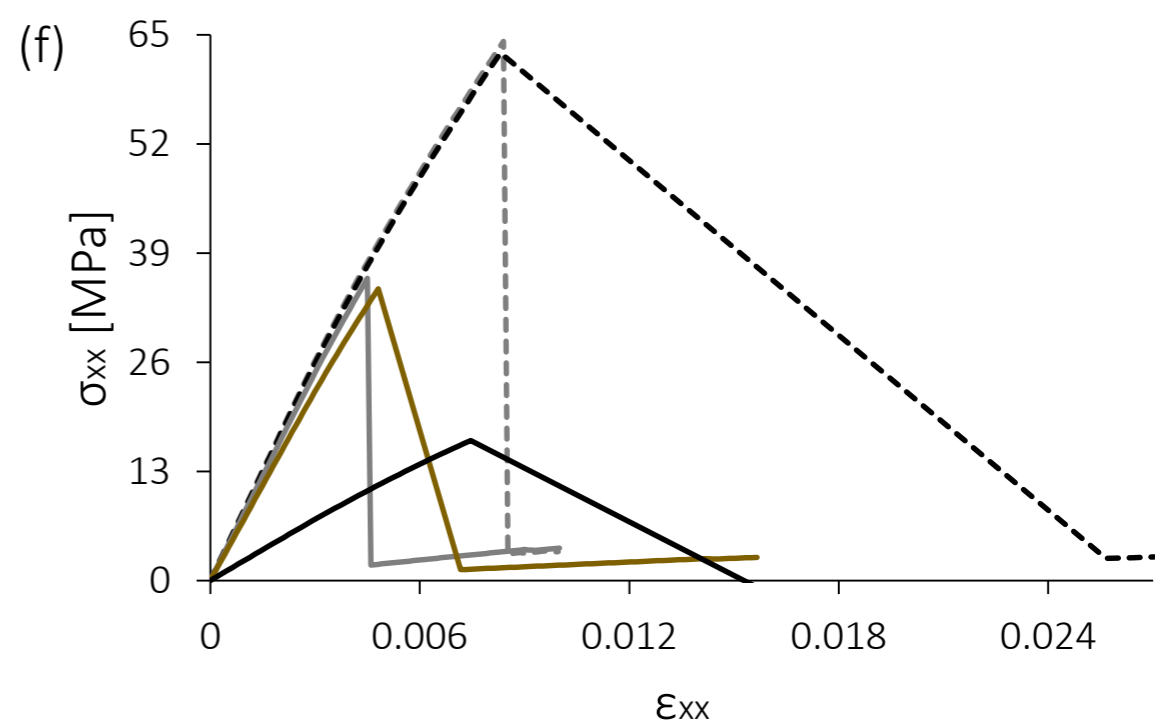
Figure(s)



Figure(s)

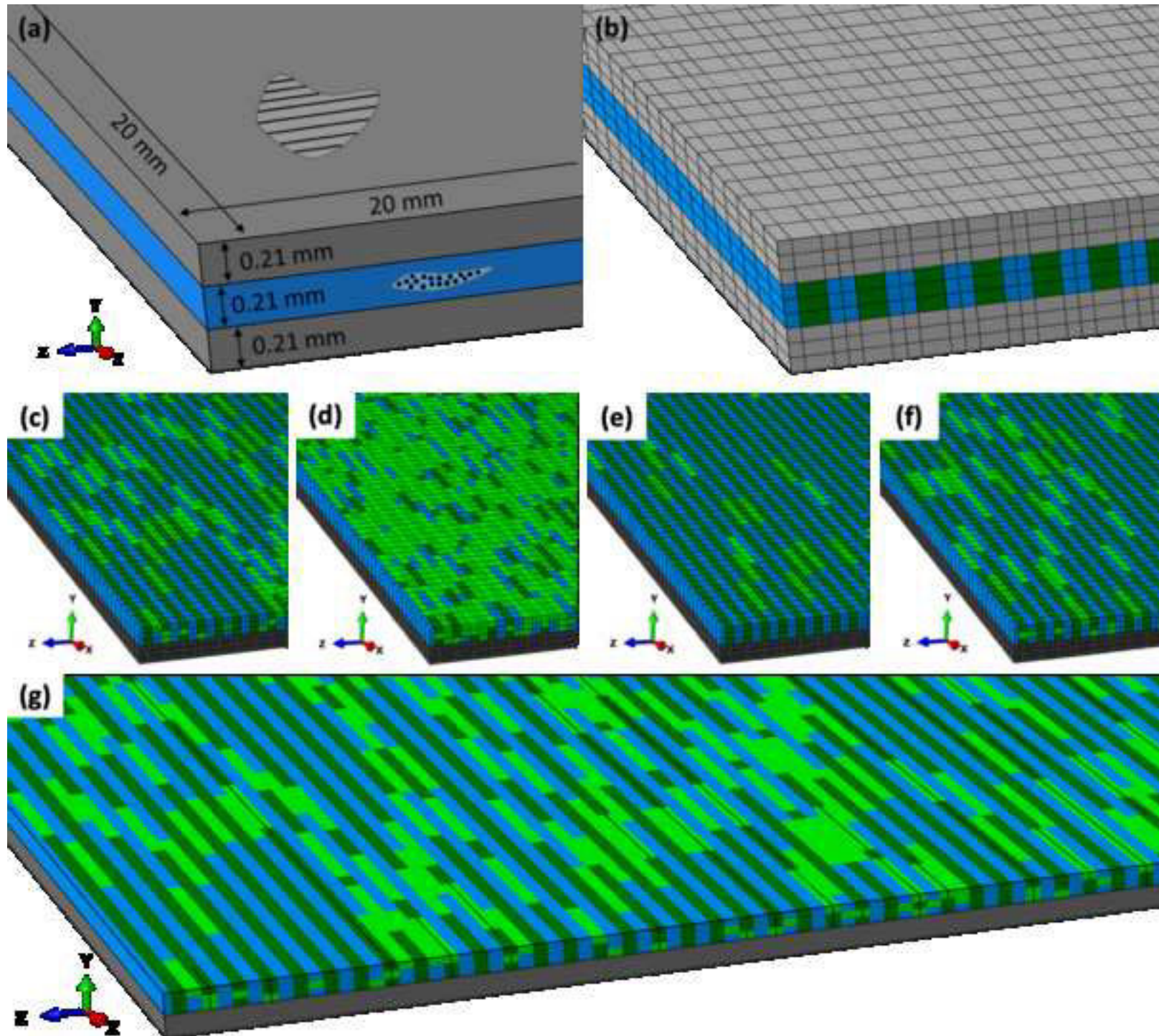


--- *E-Ref-S*    --- *D-Ref-S*    — *E-S-Low%*    — *E-S-High%*    — *D-S*

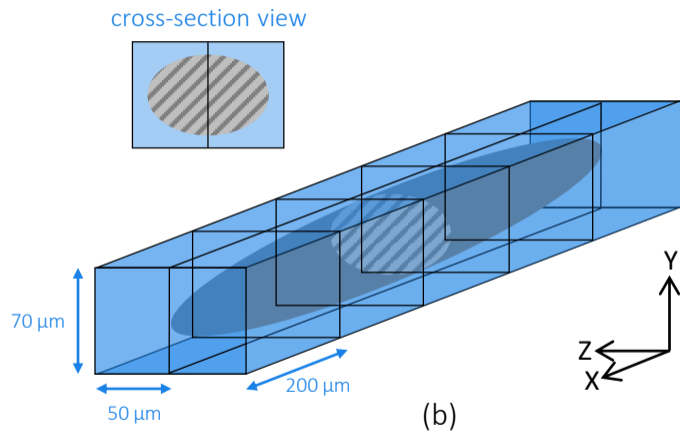
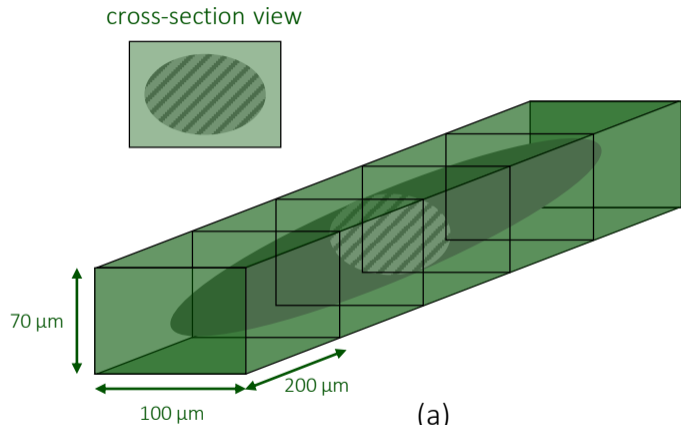


--- *E-Ref-L*    --- *D-Ref-L*    — *E-L-Low%*    — *E-L-High%*    — *D-L*

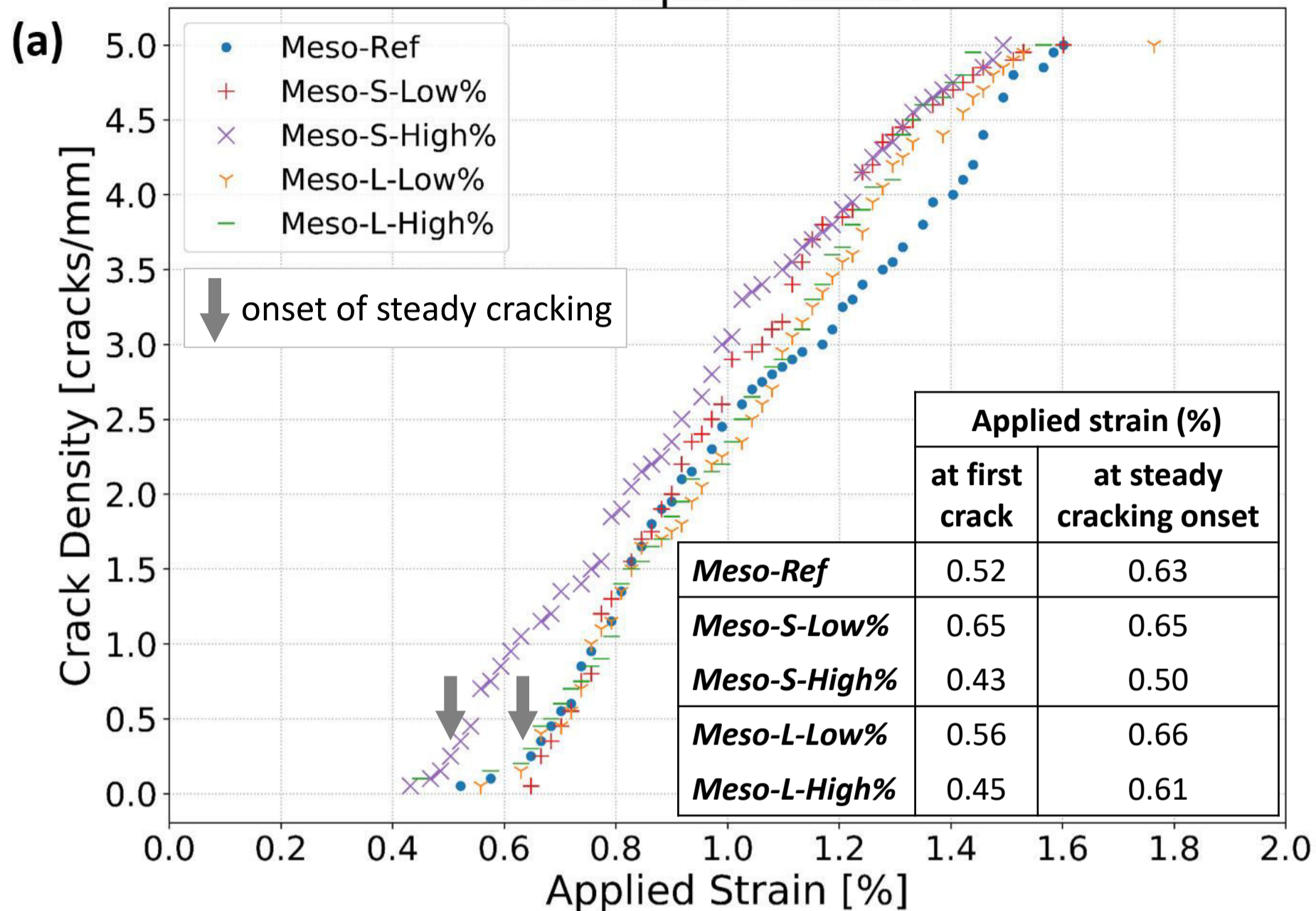
Figure(s)  
[Click here to download high resolution image](#)



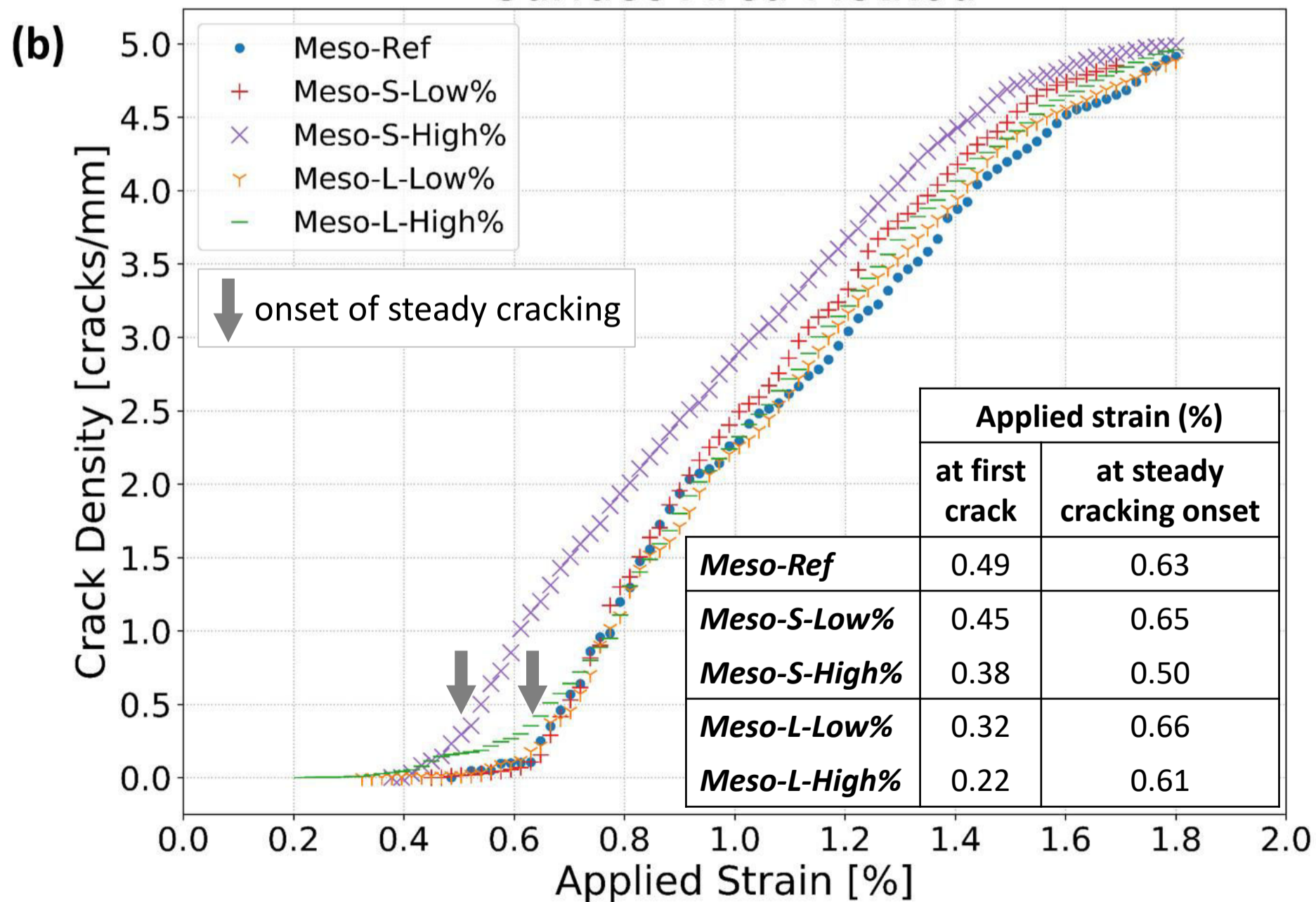
Figure(s)



## Half-Span Method



## Surface Area Method





Figure(s)

[Click here to download high resolution image](#)

